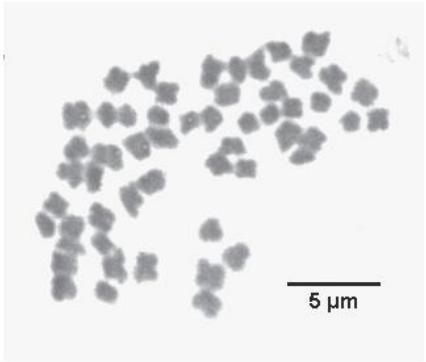

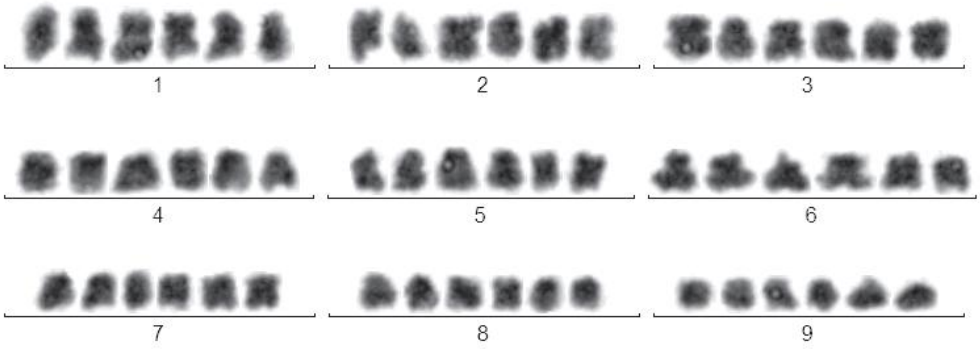

Supplementary Fig. 1 | Chromosome number of *D. sanguinalis* accession YJ2023. Acetocarmine-stained root tip cells show that the accession YJ2023 possesses 54 chromosomes (2n = 54).

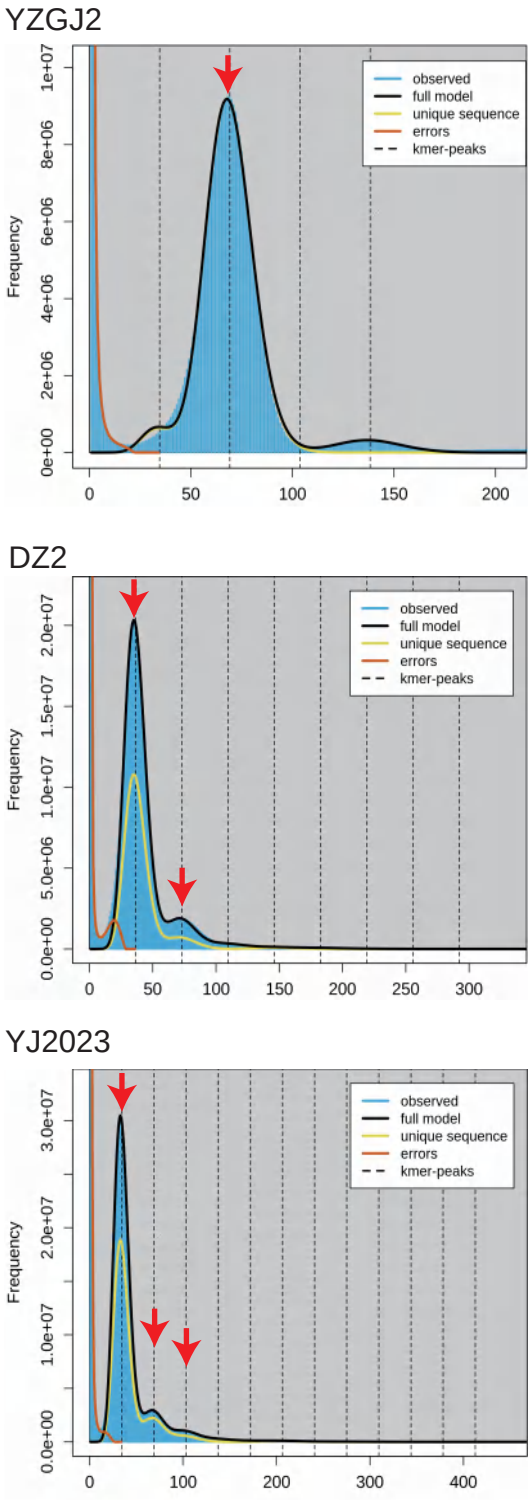

Supplementary Fig. 2 | Genome size estimation of *D. radicosa, D. milanjiana and D. sanguinalis* using *k*-mer distribution. The 21-mer frequency distribution was generated from Illumina reads for each *Digitaria* species. Genome size was estimated by calculating *(total k-mer count − unique k-mers)/peak k-mer depth*, resulting in genome sizes of 398.99 Mb (*D. radicosa*), 791.42 Mb (*D. milanjiana*), and 1239.30 Mb (*D. sanguinalis*).

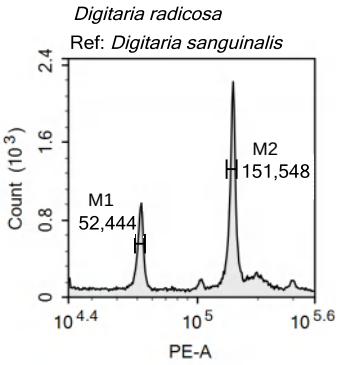

Estimated genome size: 0.47Gb

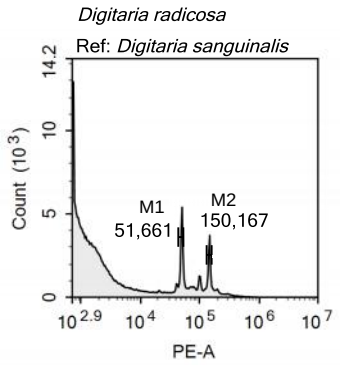

Estimated genome size: 0.46Gb

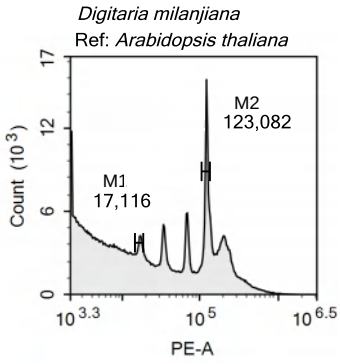

Estimated genome size: 0.90Gb

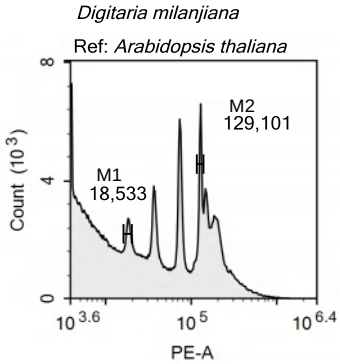

Estimated genome size: 0.87Gb

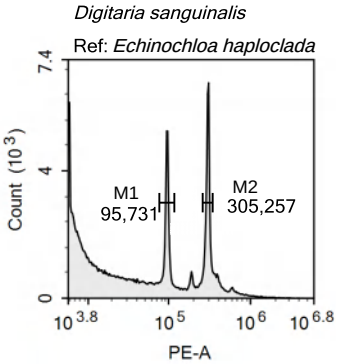

Estimated genome size: 1.34Gb

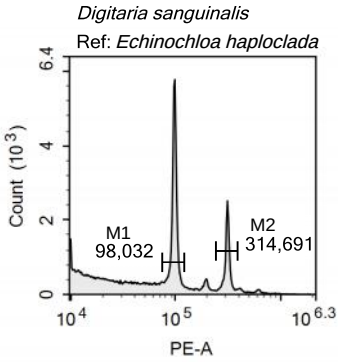

Estimated genome size: 1.35Gb

Supplementary Fig. 3 | Genome size estimation of *D. radicosa, D. milanjiana* and *D. sanguinalis* by flow cytometry. Genome sizes were estimated using flow cytometry, with internal reference standards indicated above each image.

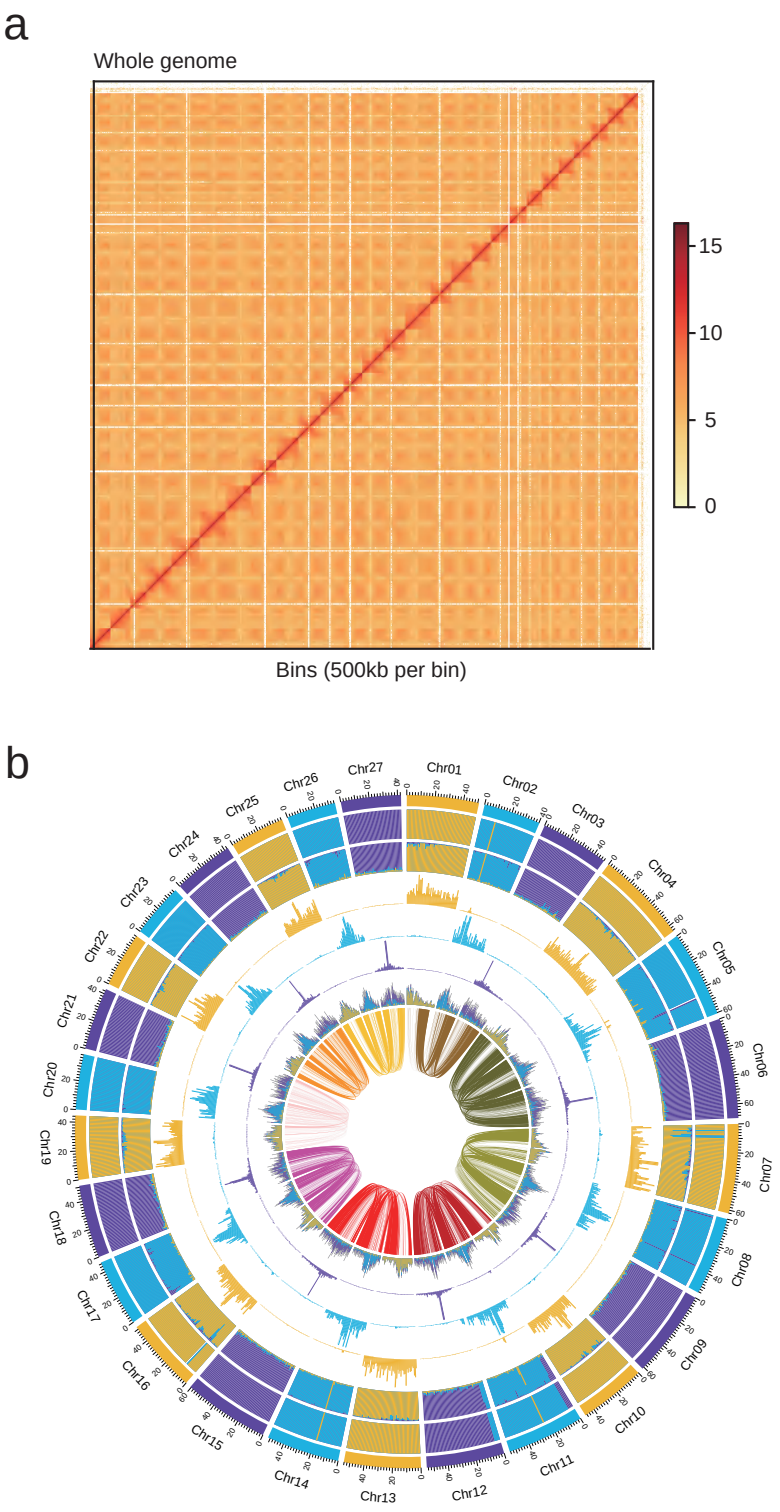

Supplementary Fig. 4 | Genome wide Hi-C interaction heatmap and subgenome phasing. a, Hi-C contact heatmap illustrating interaction frequencies, with color gradients from light yellow (low) to dark red (high). **b,** Subgenome phasing based on subgenome -specific *k*-mers. From outer to inner rings: (1) Subgenome assignment of *D. sanguinalis*; (2) Significant enrichment of subgenome-specific *k*-mers; (3) Normalized proportions of subgenome-specific *k*-mers; (4-6) Density distributions of subgenome-specific *k*-mer set; (7) Density of subgenome-specific and non-specific LTR-RTs (gray); (8) Syntenic blocks among chromosomes.

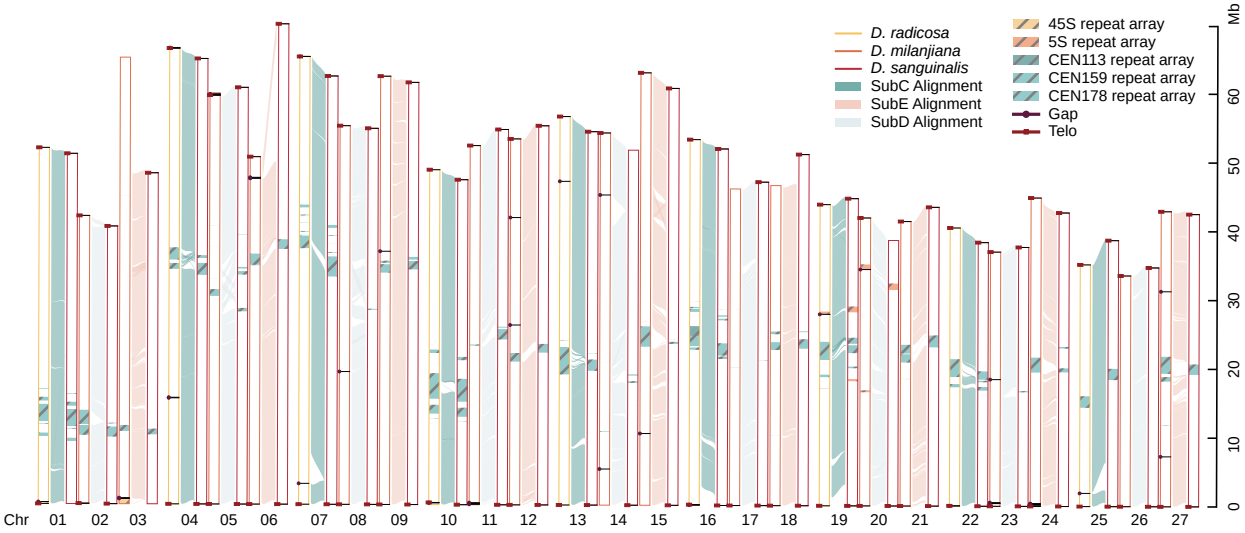

Supplementary Fig. 5 | Genomic landscape of *D. sanguinalis*, highlighting syntenic blocks among ancestral subgenomes C, D, and E. Colored blocks within species boxes denote repeat units. Gapped regions are indicated by red circles, and telomeric sequences are marked by red rectangles.

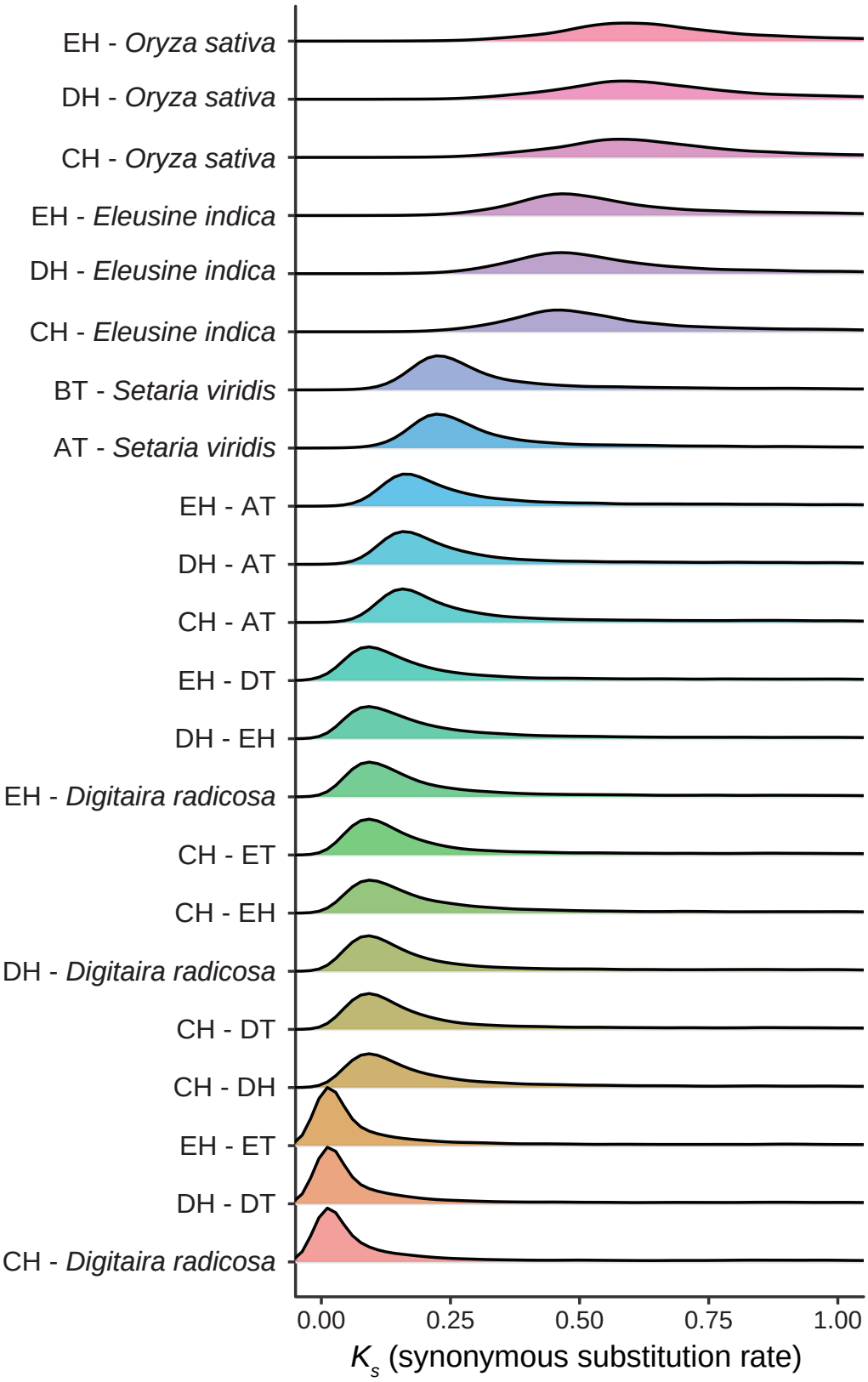

Supplementary Fig. 6 | The synonymous substitution rate (K_s) distributions of syntenic gene pairs among *Digitaria* and other genomes. Synonymous substitution rate (K_s) distributions are shown for syntenic gene pairs within *Digitaria* subgenomes and between *Digitaria* and other Poaceae (sub)genomes.

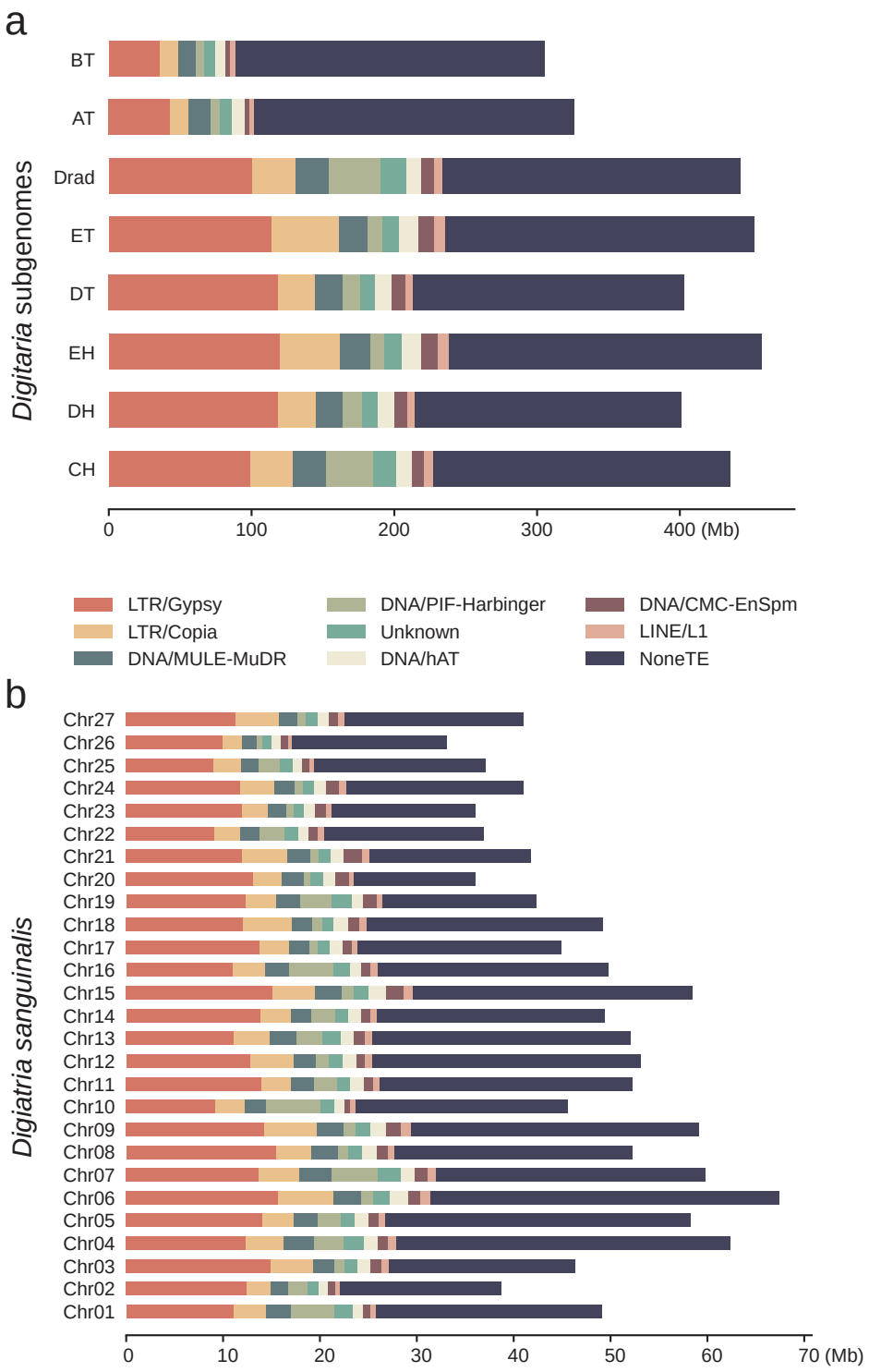

Supplementary Fig. 7 | Genomic compositions across *Digitaria* species. a, Genomic composition of each subgenome. **b,** Genomic composition across individual chromosomes in *D. sanguinalis*. Abbreviations: Drad, diploid *D. radicosa*; AT and BT, subgenomes of tetraploid *D. exilis*; DT and ET, subgenomes of tetraploid *D. milanjiana*; CH, DH, and EH, subgenomes of hexaploidy *D. sanguinalis*.

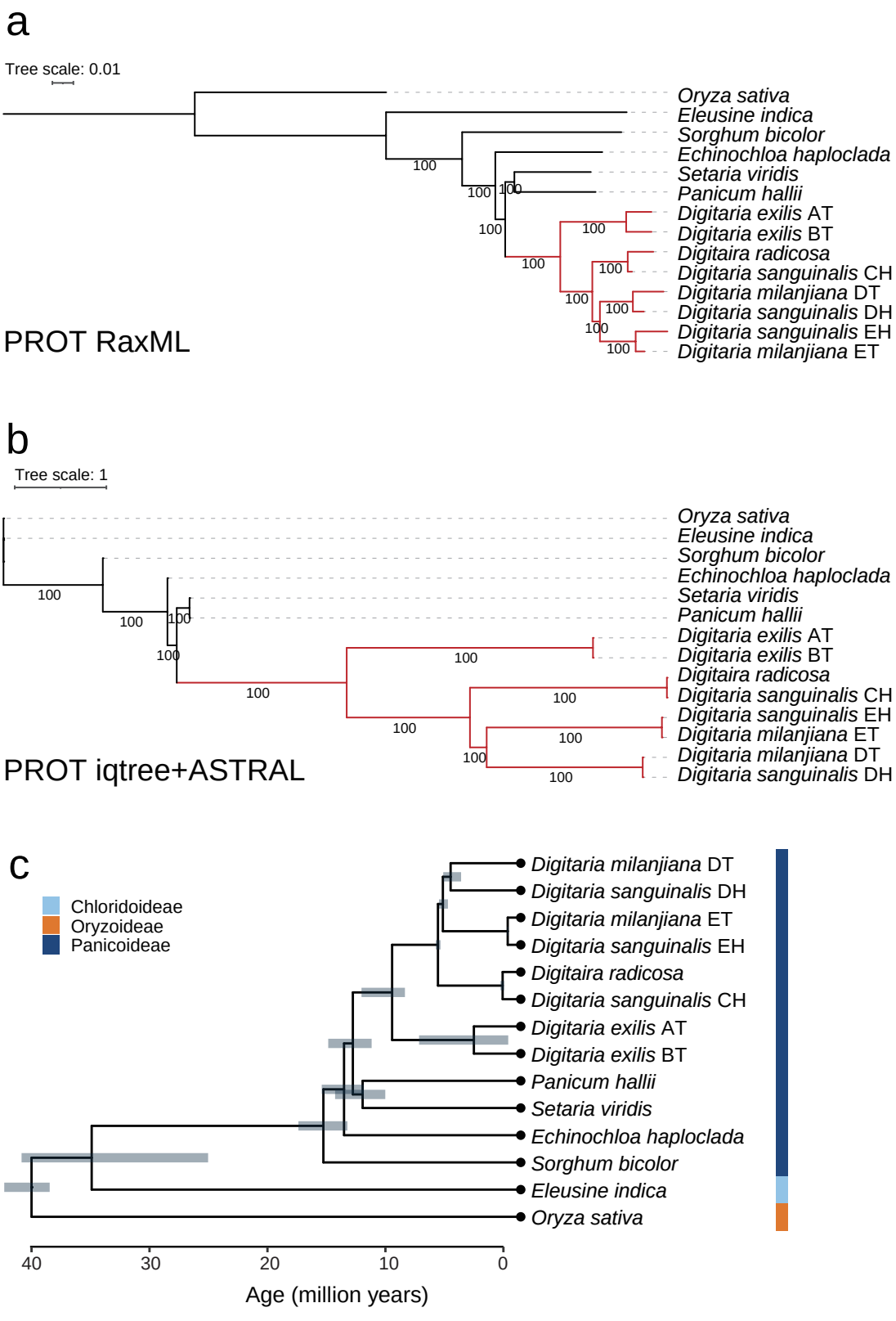

Supplementary Fig. 8 | Phylogenetic inference of *Digitaria* based on single-copy genes. a, Maximum-likelihood phylogenetic tree inferred using RAxML with the GAMMA+JTT+F4 substitution model. **b,** Phylogenetic tree constructed using IQ-TREE (best-fit model selected by ModelFinder) and ASTRAL based on 2,030 single-copy gene trees. **c,** Ultrametric phylogenetic tree and divergence times estimated using MCMCtree. Calibration was performed using fossil divergence times (41-52 Mya) between *Oryza sativa.*

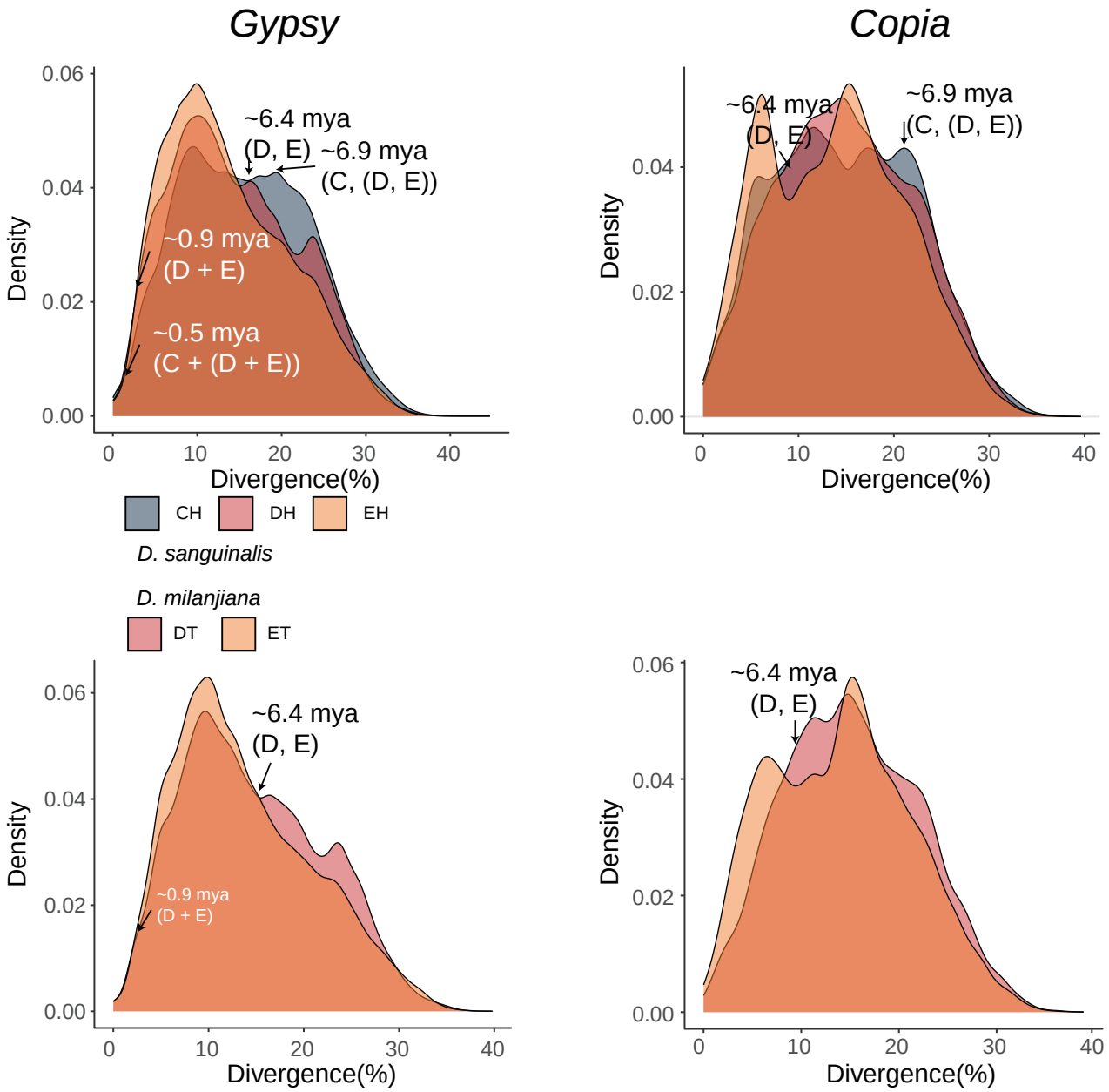

Supplementary Fig. 9 | Divergence time estimates based on transposable element divergence in *Digitaria* polyploids. Repeat elements in each subgenome were annotated using RepeatMasker. Divergence was assessed by PercDiv (percentage of nucleotide substitutions in repeat regions compared to consensus sequences). mya, million years ago.

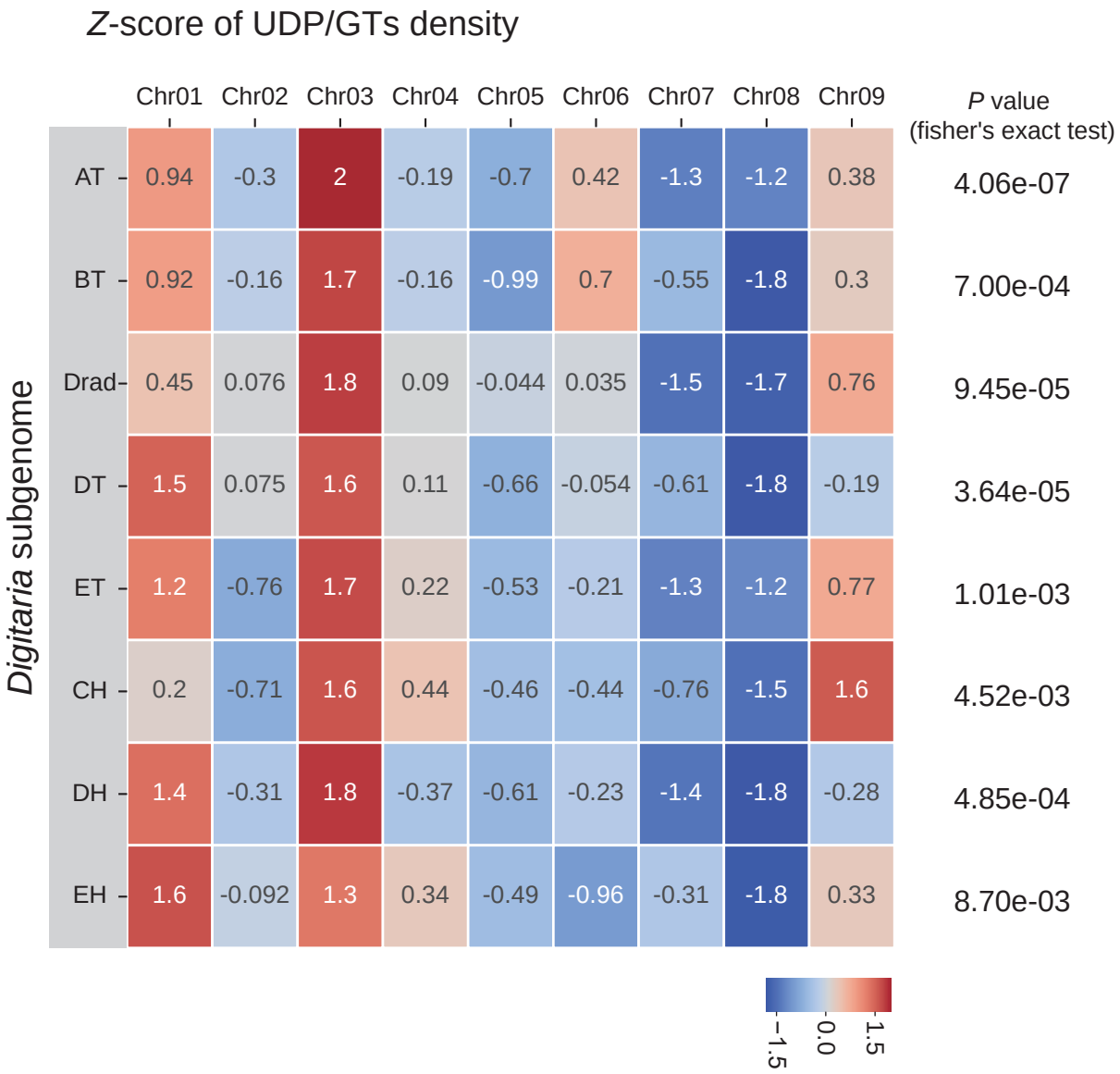

Supplementary Fig. 10 | Enrichment of UDP-glycosyltransferase (UDP/GT) genes in *Digitaria*. Gene densities across all chromosomes from each subgenome were normalized using *Z*-scores. Statistical significance was assessed using Fisher's exact test.

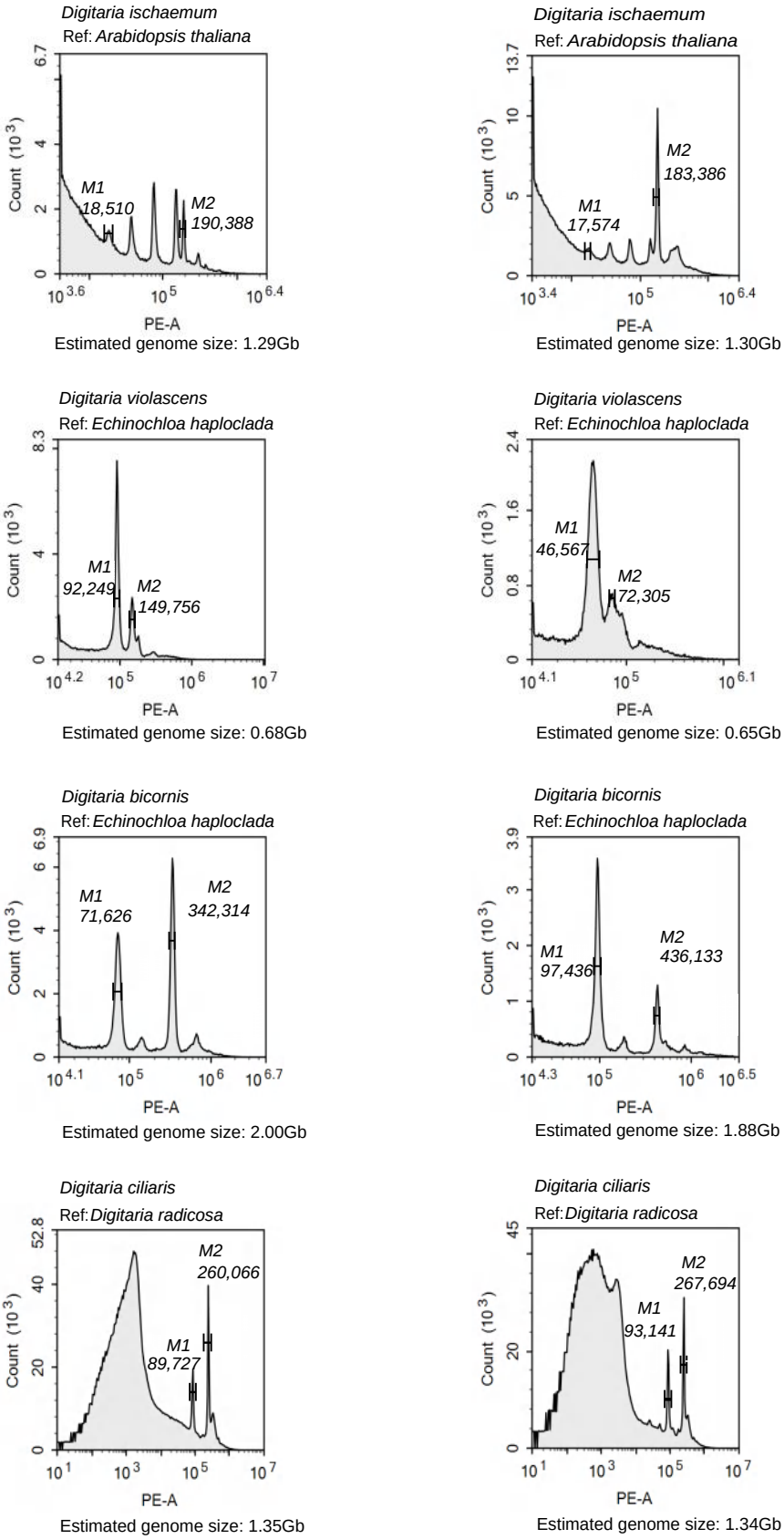

Supplementary Fig. 11 | Flow cytometric estimation of genome sizes in *D. ischaemum, D. violascens, D. bicornis,* and *D. ciliaris.* Genome sizes were estimated using flow cytometry, with internal reference standards labeled above each image.

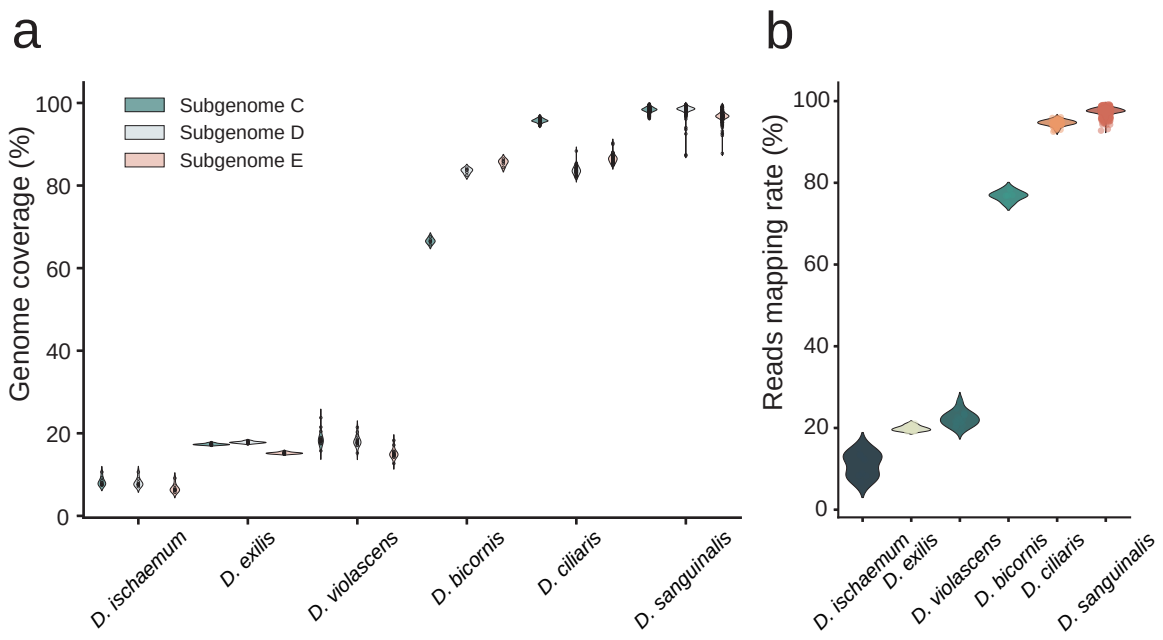

Supplementary Fig. 12 | Reads mapping of 579 re-sequenced *Digitaria* accessions to the *D. sanguinalis* reference genome (YJ2023). Genome coverage of subgenome C, D and E **(a)** and reads mapping rate **(b)** for six species (*D. ischaemum, D. violascens, D. exilis, D. bicornis, D. ciliaris* and *D. sanguinalis*).

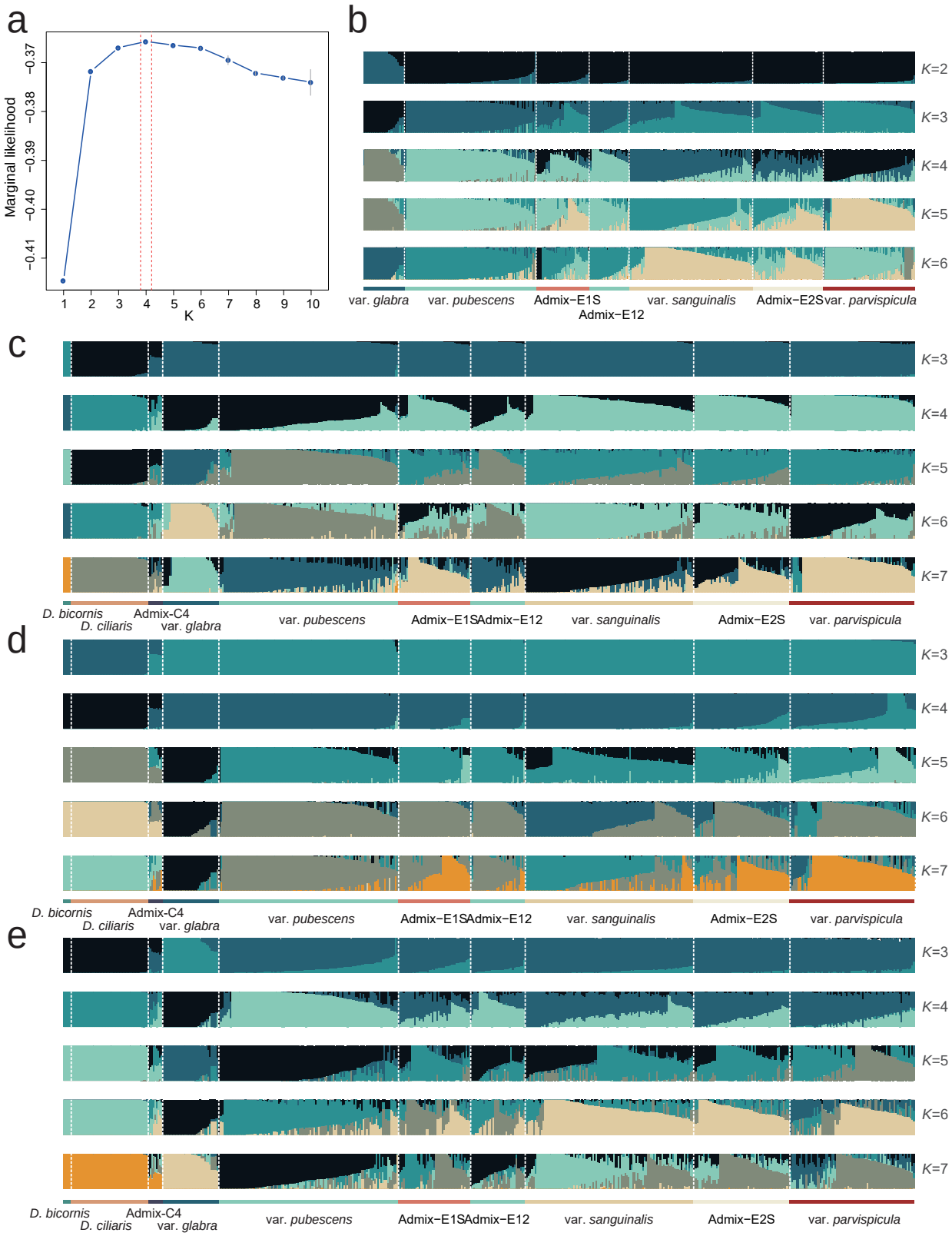

Supplementary Fig. 13 | Population structure based on whole-subgenome SNPs. **a,** Marginal likelihood plot for the unsupervised fastStructure analysis. **b,** Population structures of *D. sanguinalis* individuals from *k* = 2 to *k* = 6. **c-e,** Subgenome-specific population structures for subgenomes C **(c)**, D **(d)**, and E **(e)** across *Digitaria* species.

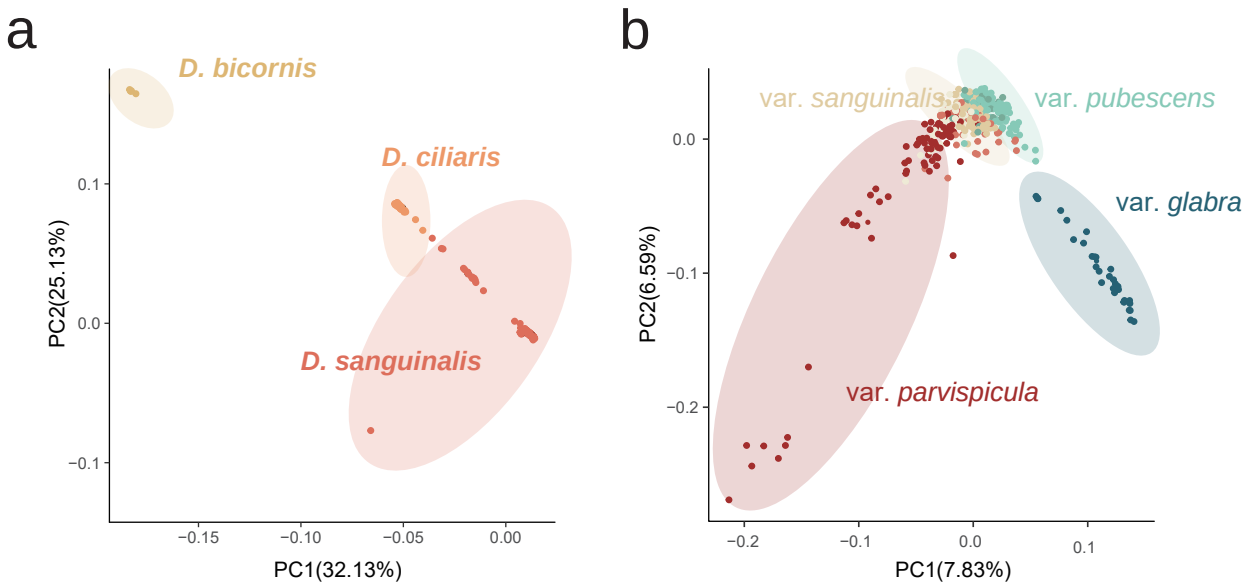

Supplementary Fig. 14 | Principal component analysis (PCA) of *Digitaria* accessions. **a,** PCA of all binate *Digitaria* individuals. **b,** PCA of *D. sanguinalis* individuals, based on whole-genome pruned SNPs.

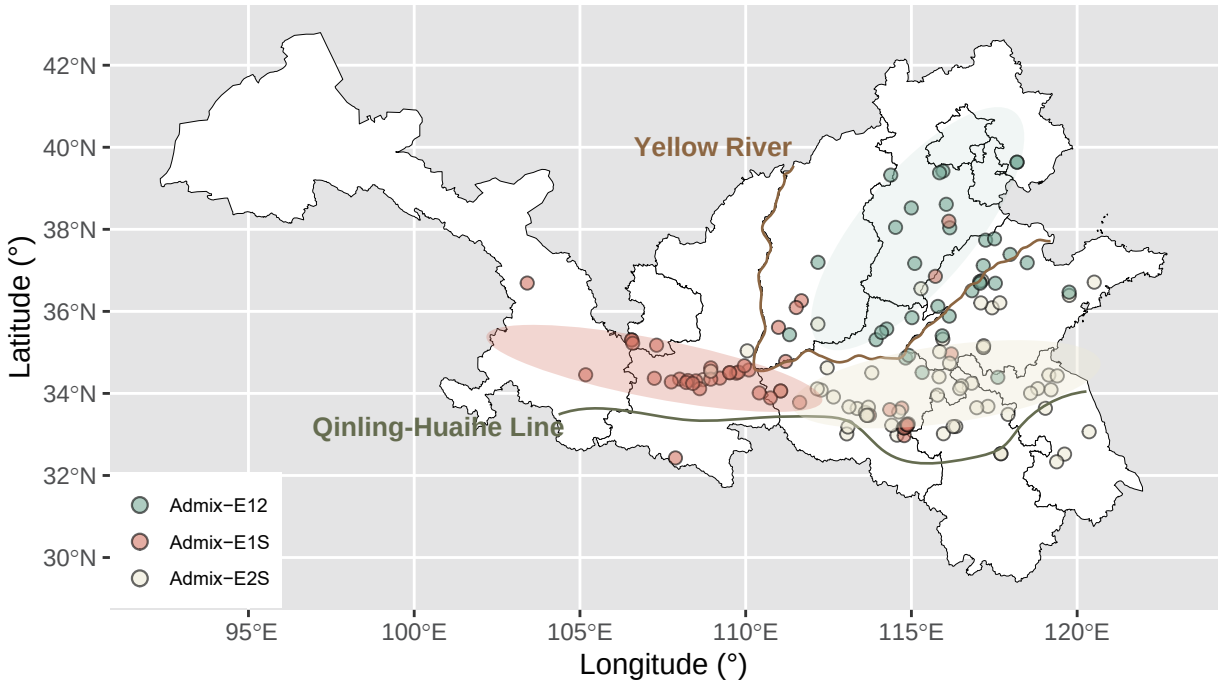

Supplementary Fig. 15 | Geographic distribution of admixed *D. sanguinalis* accessions. Primary distribution areas of admixed accessions are indicated by colored blocks. Key hydrogeographic boundaries are annotated on the map.

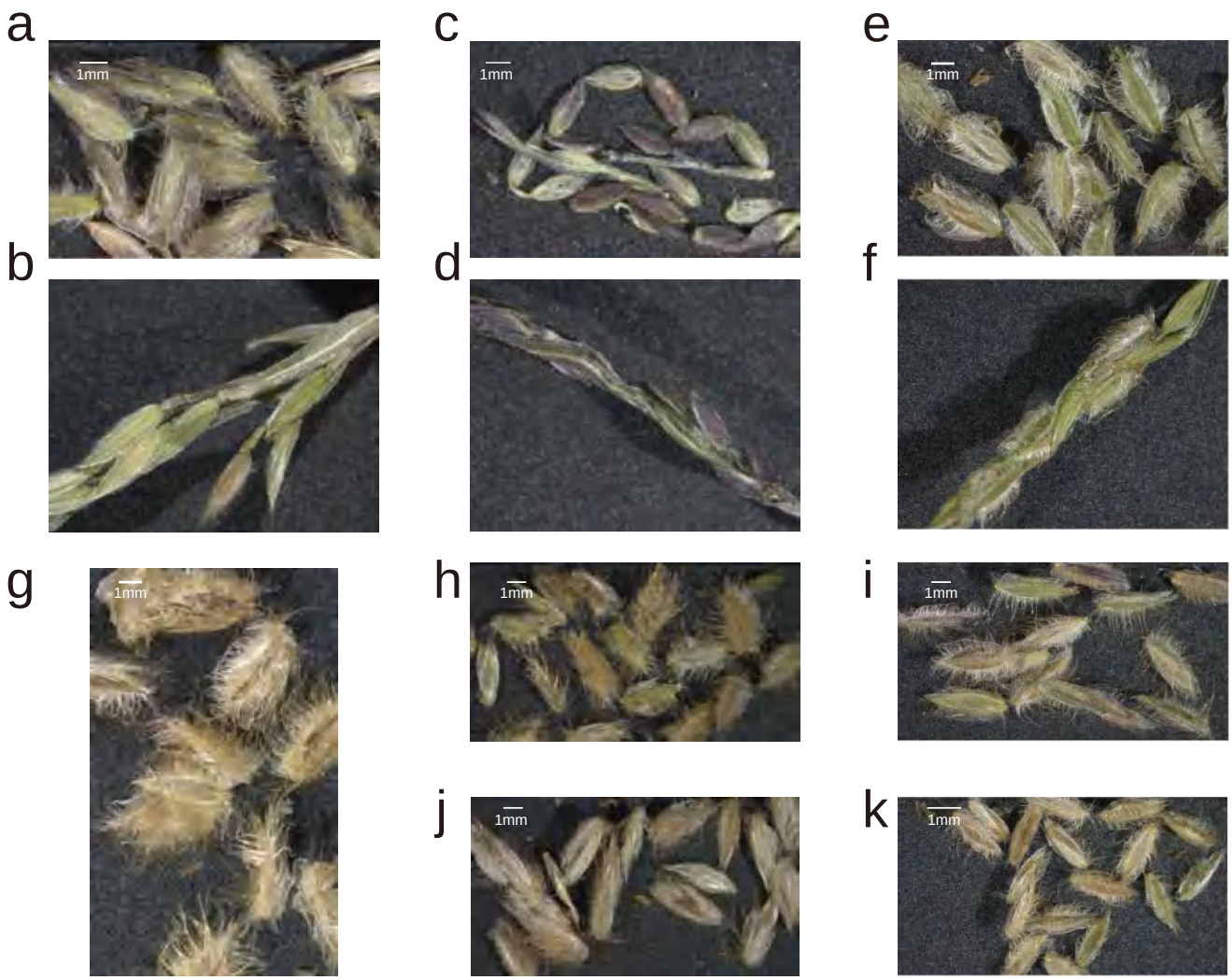

Supplementary Fig. 16 | Spikelet phenotypes of *Digitaria* species. a, *D. ischaemum*. Panicle of *D. ischaemum* **(b)** and *D. violascens* **(d)** exhibits trifurcate spikelets. **c,** *D. violascens*. **e,** *D. bicornis*. **f,** A characteristic bifurcate spikelets in *D. bicornis* panicle, with basal spikelets being slender and glabrous. **g,** *D. ciliaris*. **h,** *D. sanguinalis* var. *pubescens*. **i,** *D. sanguinalis* var. *sanguinalis*. **j,** *D. sanguinalis* var. *glabra*. **k,** *D. sanguinalis* var. *parvispicula*.

Supplementary Fig. 17 | Plant architectures of *Digitaria* species in this study. a, *D. ischaemum*. **b,** *D. violascens*. **c,** *D. bicornis*. **d,** *D. ciliaris*.

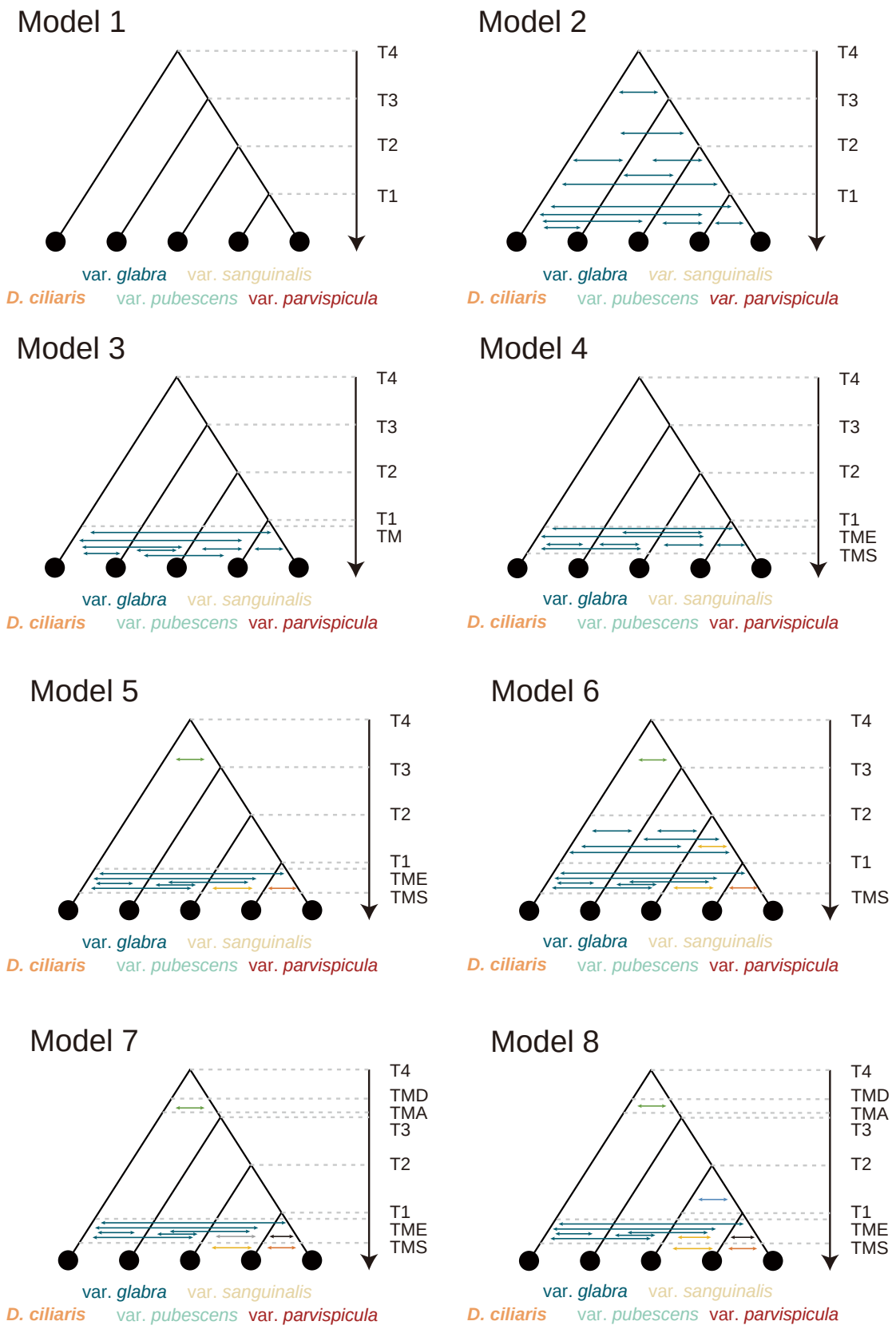

Supplementary Fig. 18 | Eight hypothetical scenarios for divergence of four *D. sanguinalis* varieties with *D. bicornis* as an outgroup. var. *pubescens*, *D. sanguinalis* var. *pubescens*. var. *sanguinalis*, *D. sanguinalis* var. *sanguinalis*. var. *glabra*, *D. sanguinalis* var. *glabra*. var. *parvispicula*, *D. sanguinalis* var. *parvispicula*.

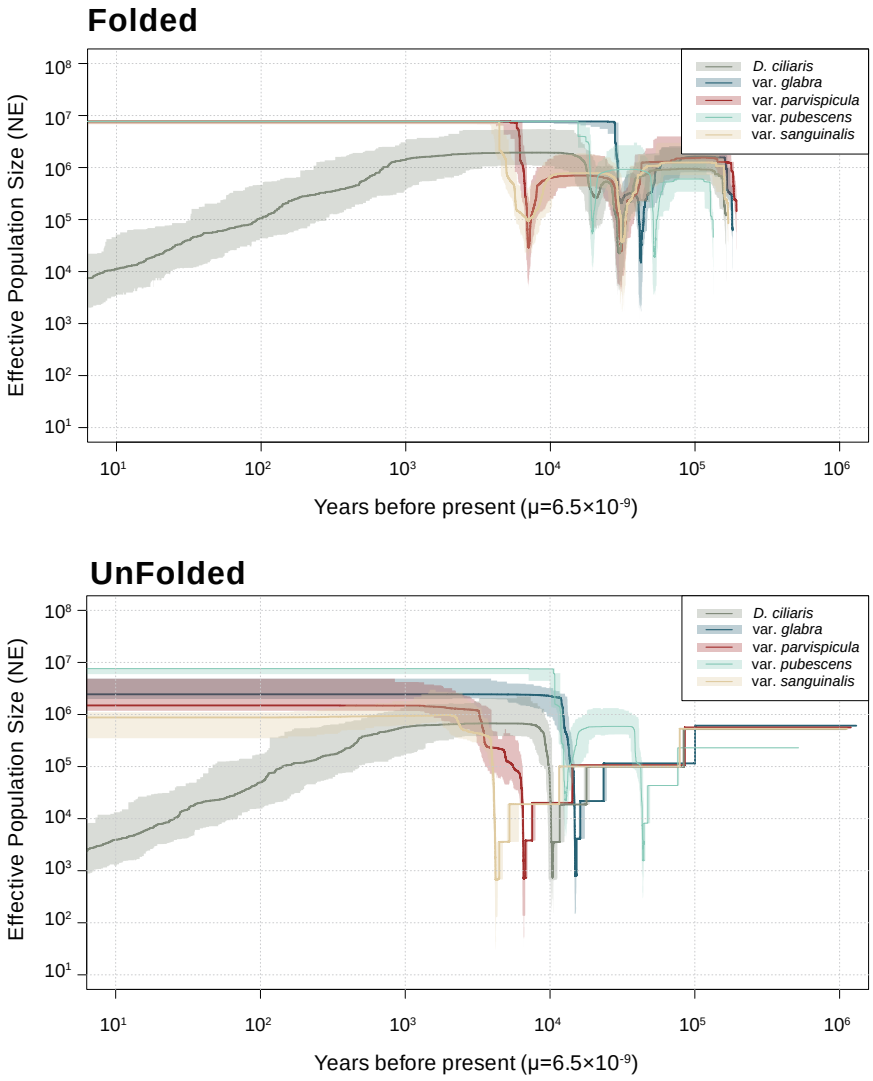

Supplementary Fig. 19 | Recent demographic history of *D. sanguinalis* varieties and *D. ciliaris* inferred by Stairway Plot using folded SFS (a) and unfolded SFS (b). The line indicates the median of effective population size N_e estimation based on 200 inferences, and the error band indicates 95% confidence interval for each population.

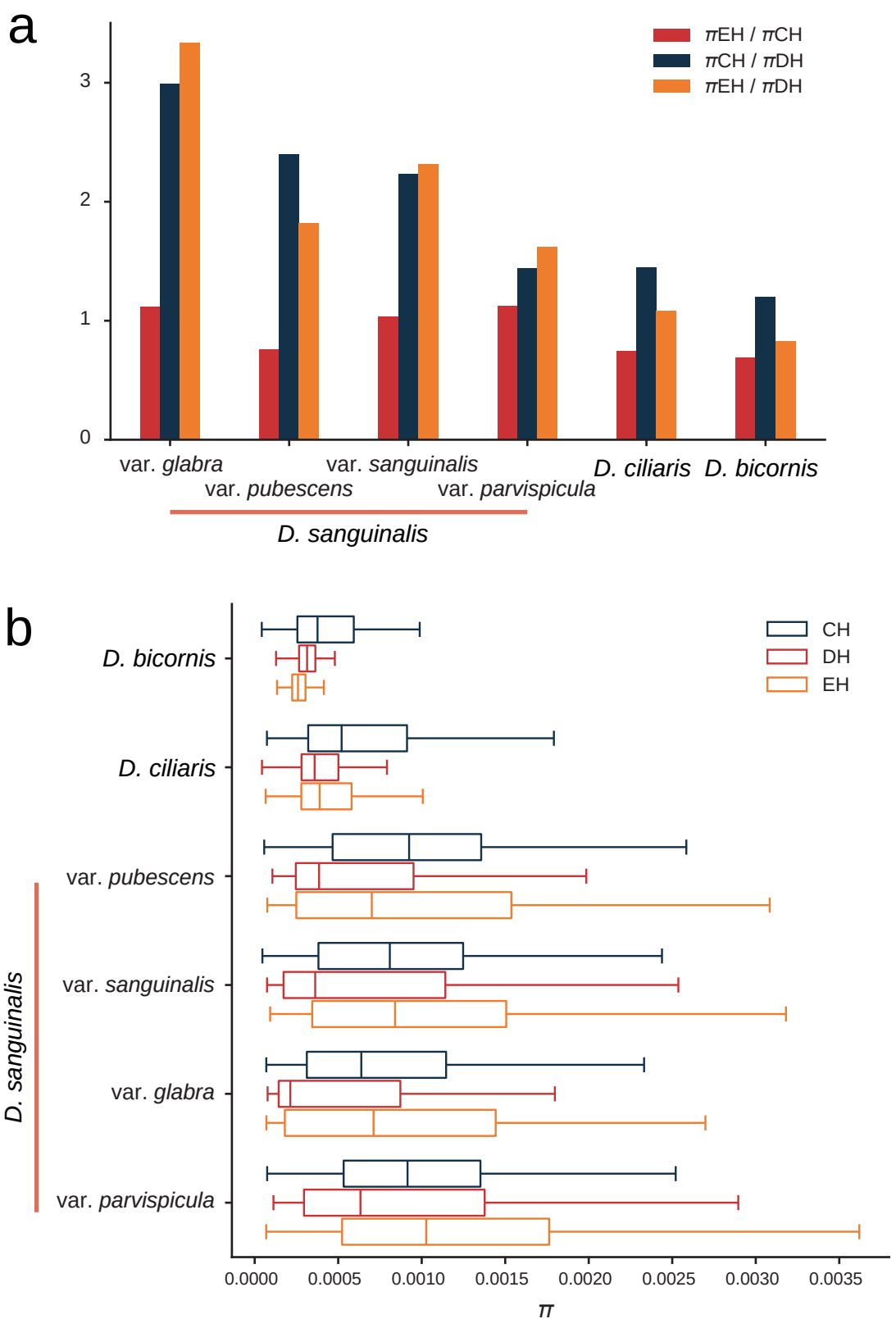

Supplementary Fig. 20 | Genome-wide nucleotide diversity (π) in *Digitaria*. a, Comparison of nucleotide diversity among subgenomes in binate *Digitaria* accessions. **b,** Nucleotide diversity in species and varieties at the subgenome level. 100-kb sliding windows: *n* = 9,063 for CH, *n* = 8,396 or DH, *n* = 9,499 for EH. In the box plots, the vertical line shows the median value, and the whiskers show the 25% and 75% quartile values.

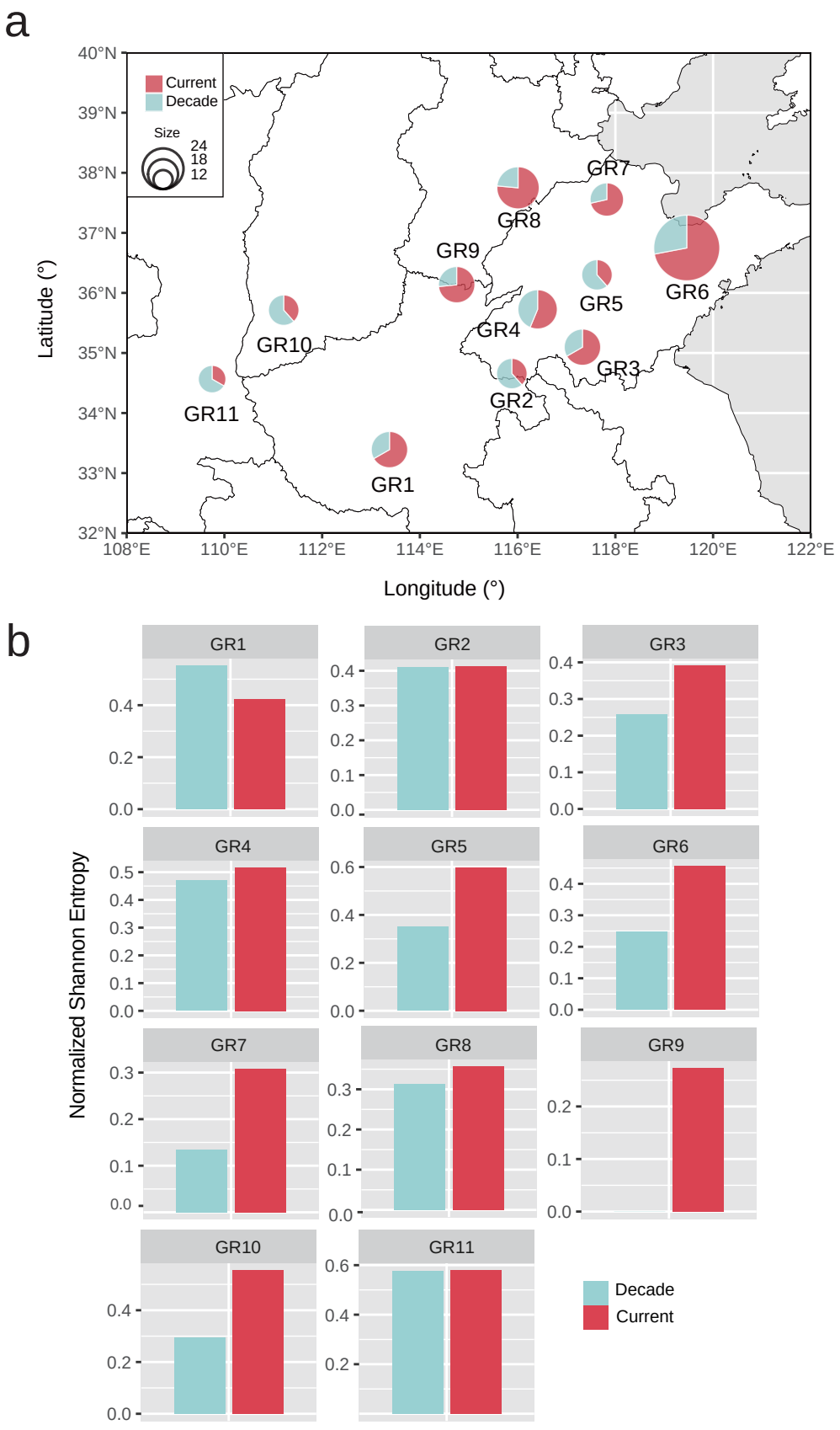

Supplementary Fig. 21 | Spatiotemporal *Digitaria* population distribution and genetic biodiversity across geographic ranges. a, Spatial and temporal distribution of accessions. Circle size indicates number of accessions; colors differentiate historical (2013 and 2015) and modern collections (2023). **b,** Normalized Shannon entropy within spatial and temporal population groups.

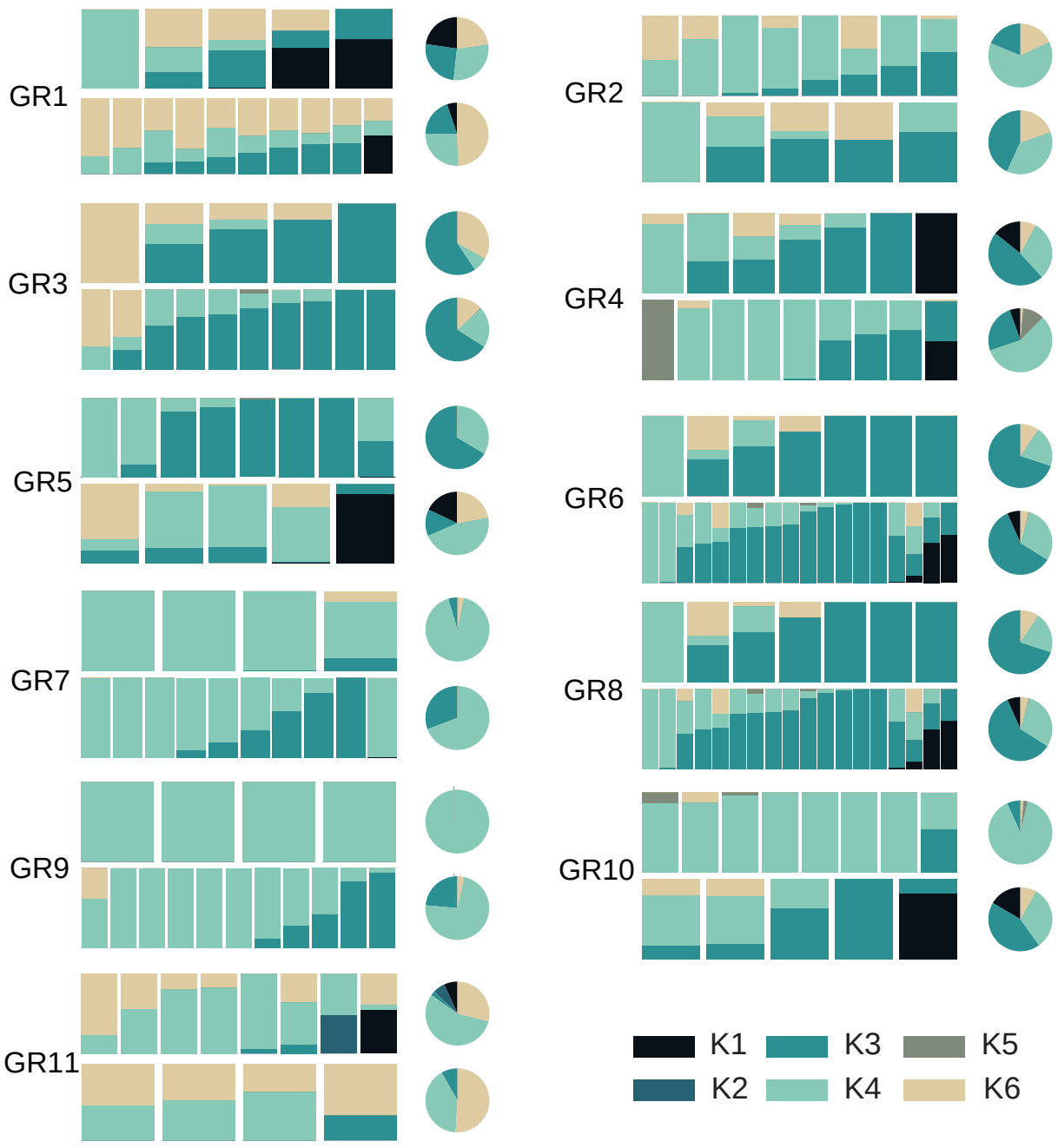

Supplementary Fig. 22 | Admixture analysis of spatial groups at *k* = 6. Bar plots show individual ancestry proportions; the accompanying pie chart illustrates overall component proportions across groups.

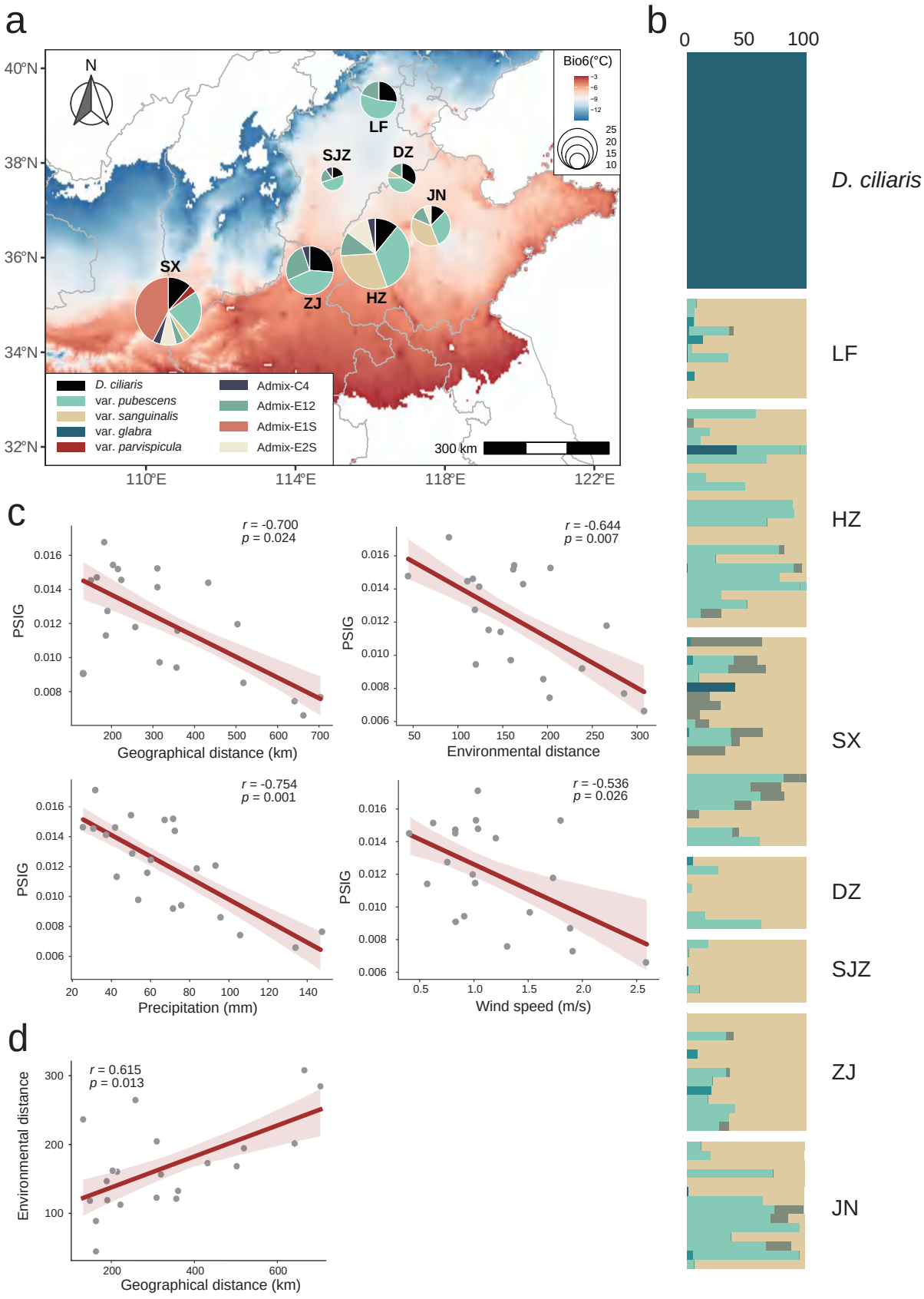

Supplementary Fig. 23 | Genome-wide introgression analysis between sympatric *D. ciliaris* and *D. sanguinalis*. a, Natural distribution of sympatric groups, colored by species. Colors reflect variation in minimum temperature of the coldest month (Bio6). **b,** Population structure at $k = 5$ for sympatric accessions. **c,** Mean proportion of shared introgressed genomic regions (PSIG) negatively correlates with geographic distance, environmental distance, precipitation, and wind speed. **d,** Correlation between environmental and geographic distances.

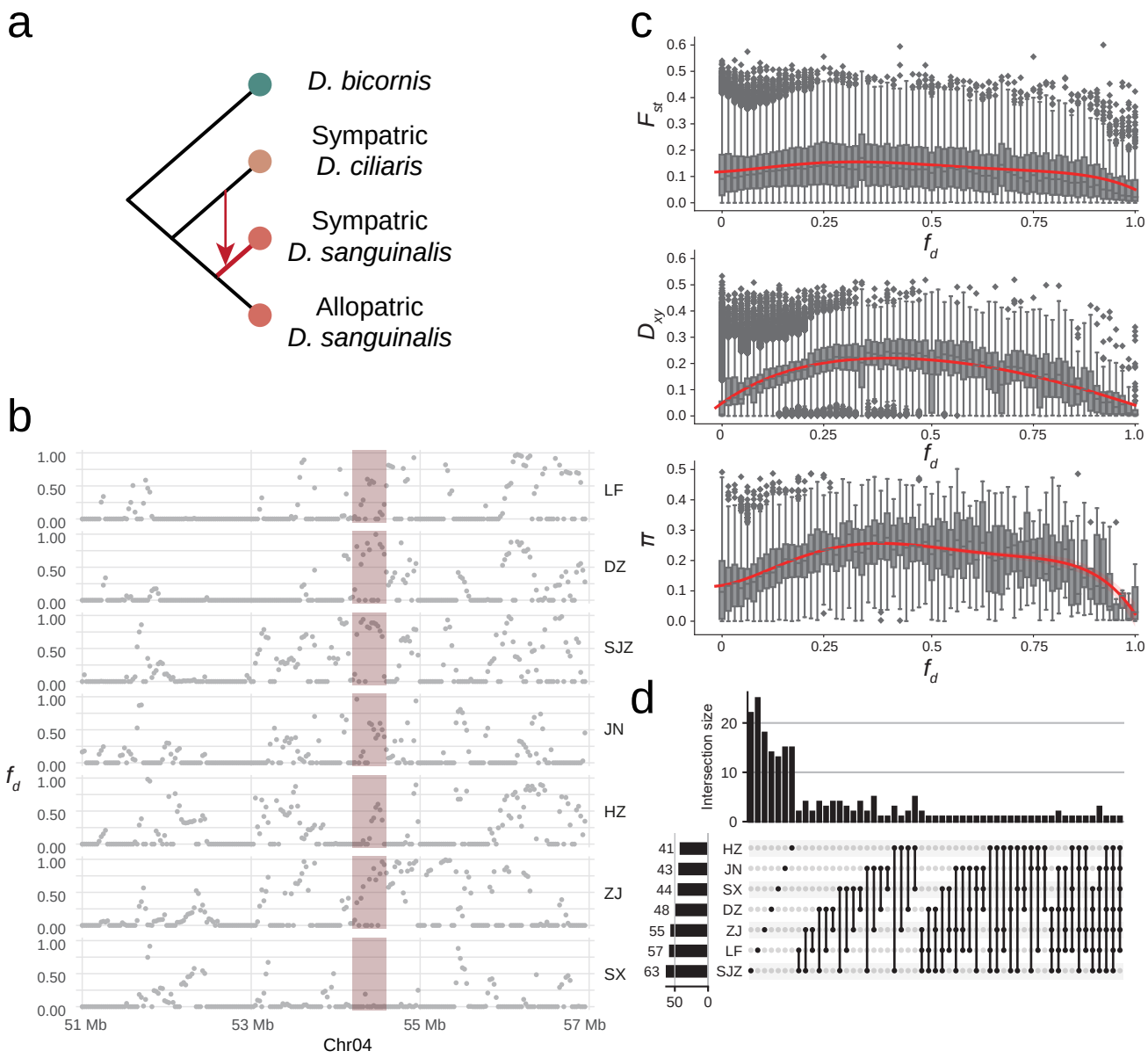

Supplementary Fig. 24 | ABBA-BABA test and genomic impact of introgression in sympatric groups. a, Illustration of ABBA-BABA topology; red arrow indicates direction of introgression from P3 to P2. **b,** Proportion of introgression f_d distributions of ABBA-BABA test on Chr4 in upper topology. Genomic regions containing SNPs significantly associated with the Bio6 are highlighted in red. **c,** Correlation among nucleotide diversity (π), fixation index (F_{st}), nucleotide diversity (D_{xy}) and introgression (f_d). f_d values were calculated using 0.01 sliding windows. In the box plots of f_d windows, the horizontal line shows the median value, and the whiskers show the 25% and 75% quartile values of diversity π. The red lines are the fitting curves between f_d and other paraments. **d,** The upSet plot represents the number of gene families in each group and the number of shared families across the groups with bar charts.

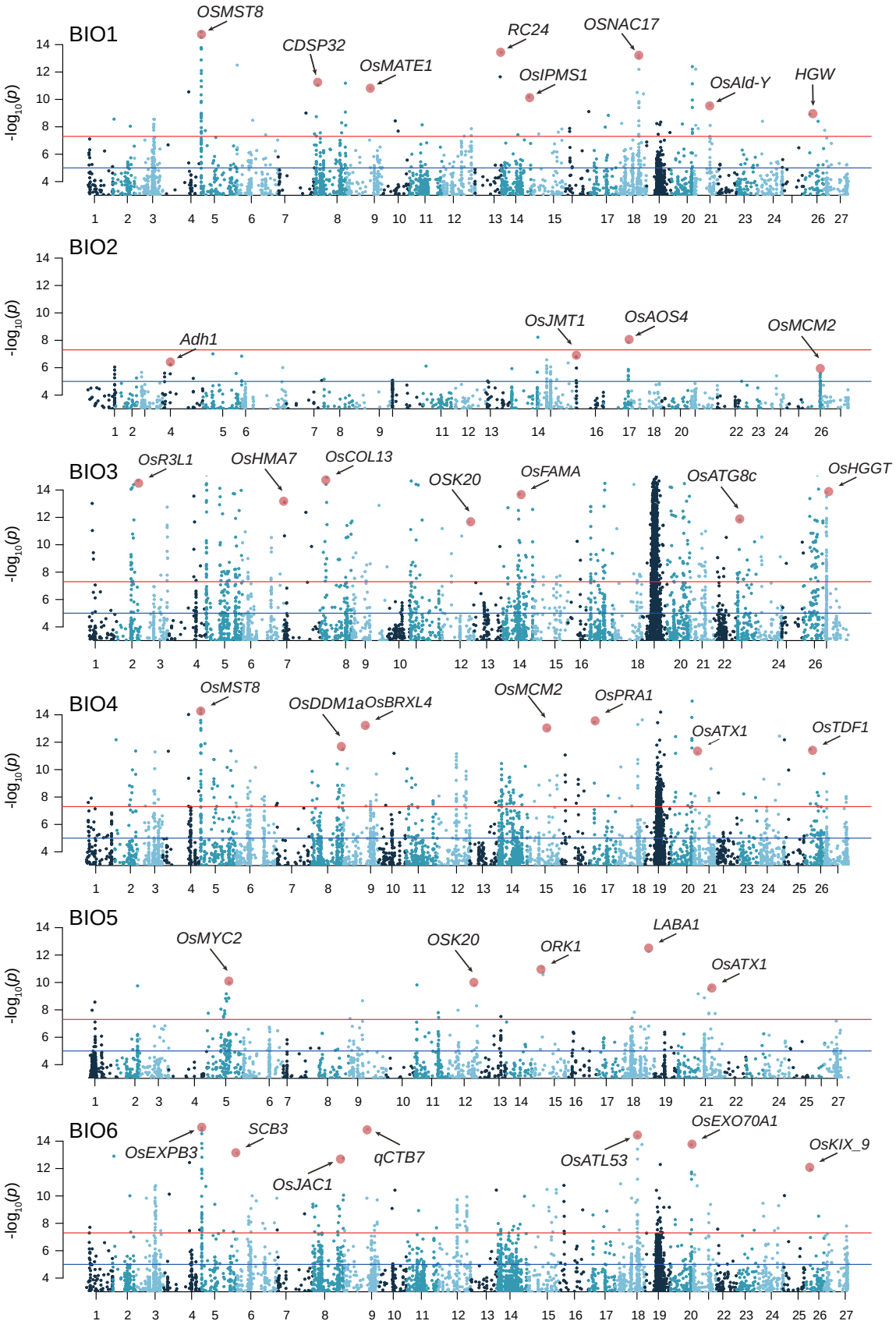
BIO1
OSMST8
CDSP32
OsMATE1
RC24
OSNAC17
OsIPMS1
OsAld-Y
HGW
BIO2
Adh1
OsJMT1
OsAOS4
OsMCM2
BIO3
OsR3L1
OsHMA7
OsCOL13
OSK20
OsFAMA
OsATG8c
OsHGGT
BIO4
OsMST8
OsDDM1a
OsBRXL4
OsMCM2
OsPRA1
OsATX1
OsTDF1
BIO5
OsMYC2
OSK20
ORK1
LABA1
OsATX1
BIO6
OsEXPB3
SCB3
OsJAC1
qCTB7
OsATL53
OsEXO70A1
OsKIX_9
-log10(p)

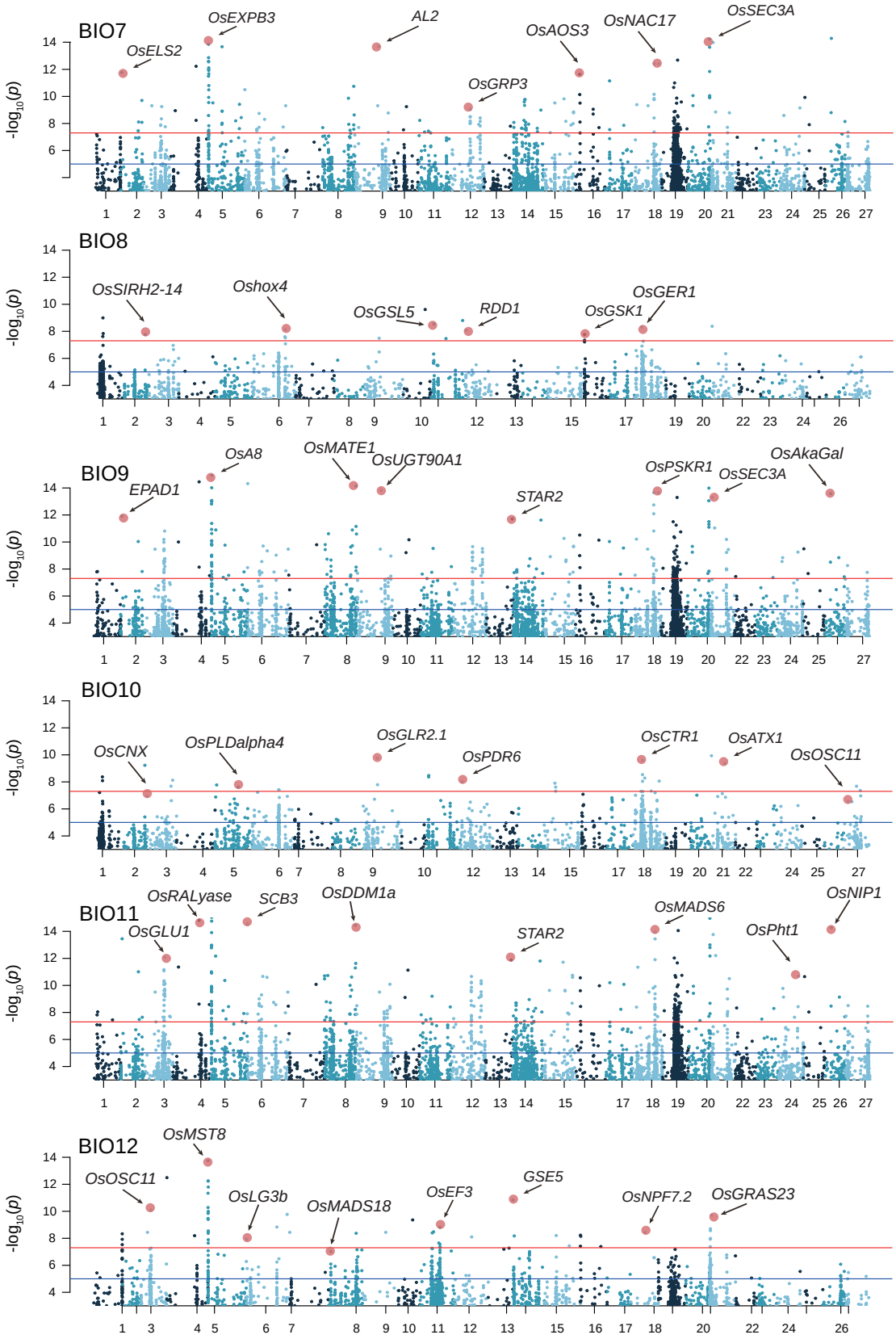
BIO7
OsEXPB3
AL2
OsAOS3
OsNAC17
OsSEC3A
OsELS2
OsGRP3
BIO8
OsSIRH2-14
Oshox4
OsGSL5
RDD1
OsGSK1
OsGER1
BIO9
OsA8
OsMATE1
OsUGT90A1
OsPSKR1
OsSEC3A
OsAkaGal
EPAD1
STAR2
BIO10
OsCNX
OsPLDalpha4
OsGLR2.1
OsPDR6
OsCTR1
OsATX1
OsOSC11
BIO11
OsRALyase
SCB3
OsDDM1a
OsMADS6
OsNIP1
OsGLU1
STAR2
OsPht1
BIO12
OsMST8
OsOSC11
OsLG3b
OsMADS18
OsEF3
GSE5
OsNPF7.2
OsGRAS23
-log10(p)

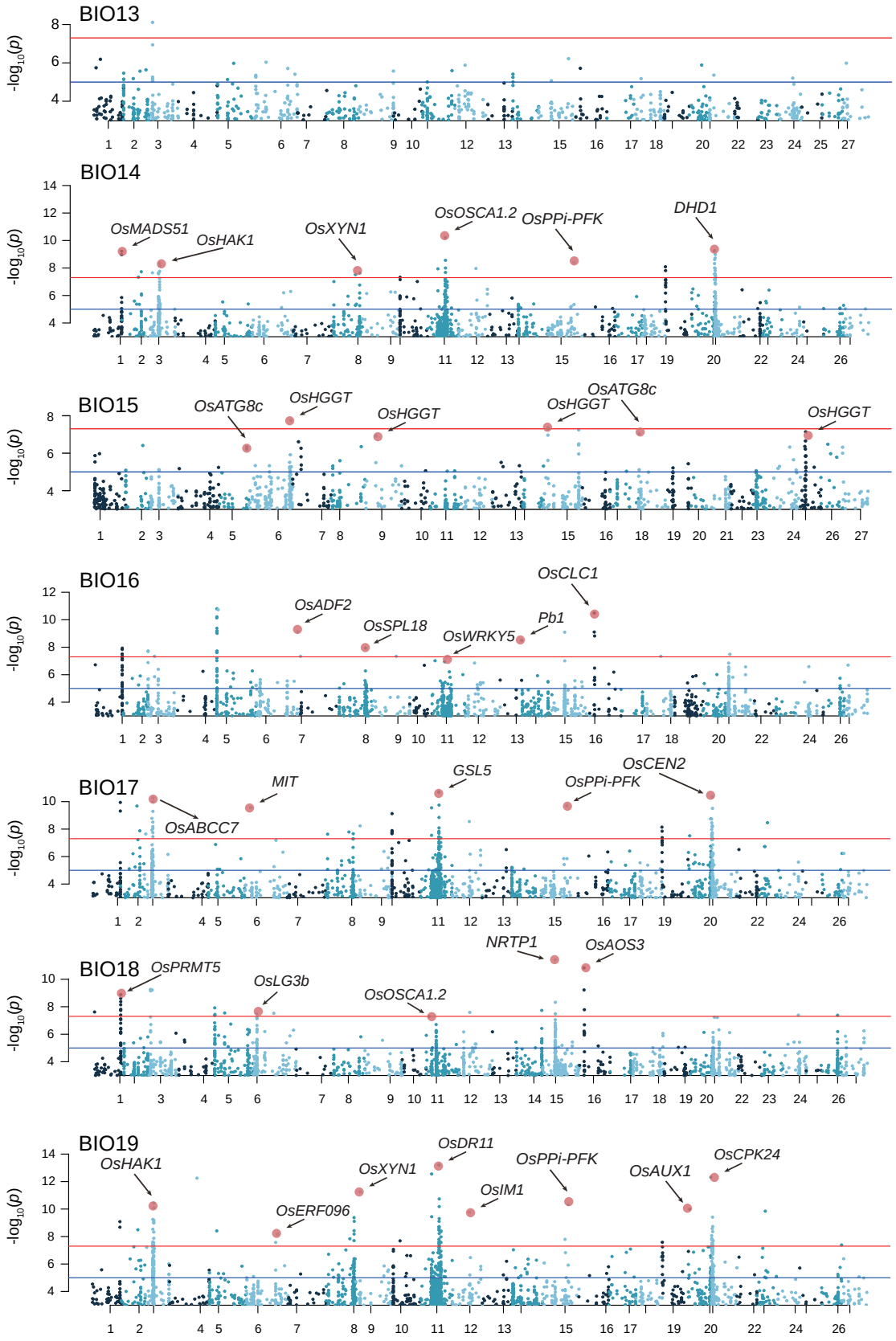

Supplementary Fig. 25 | Genome-wide associations with environmental variables. Manhattan plot shows the genotype-environment association estimated with LFMM. Two multiple comparisons methods were made: the blue line represents the 5% false discovery rate correction thresholds; red represents the Bonferroni correction, *p* value threshold of 0.05. Colors distinguish different chromosomes.

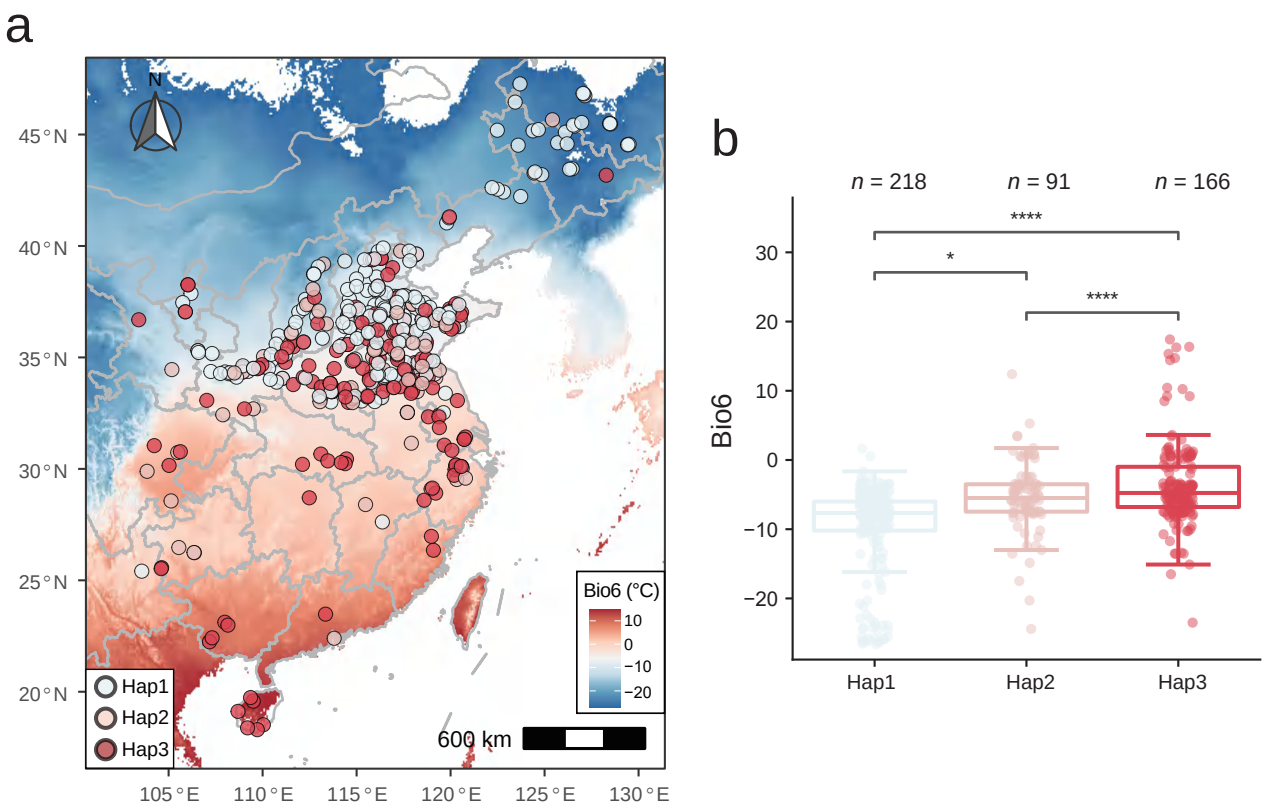

Supplementary Fig. 26 | Haplotypes distribution of *DsRZ2* across *D. sanguinalis* accessions. a, Geographic distribution of accessions across different haplotypes. **b,** Bio6 values across different haplotype accessions. In the box plots, the vertical line shows the median value, and the whiskers show the 25% and 75% quartile values. Statistical analysis of these data was performed using the two-tailed *t*-test (**p* < 0.05, ***p* < 0.01, ****p* < 0.001).

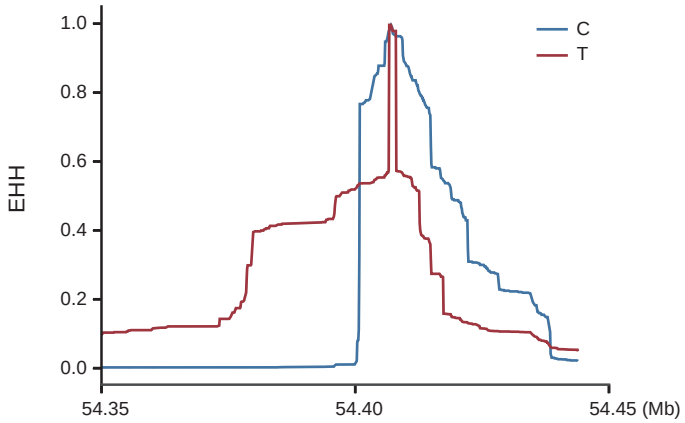

Supplementary Fig. 27 | Selection signal at *DsRZ2* locus in *D. sanguinalis*. Extended haplotype homozygosity (EHH) decay is shown for two alternative alleles surrounding Chr4: 54,407,074.

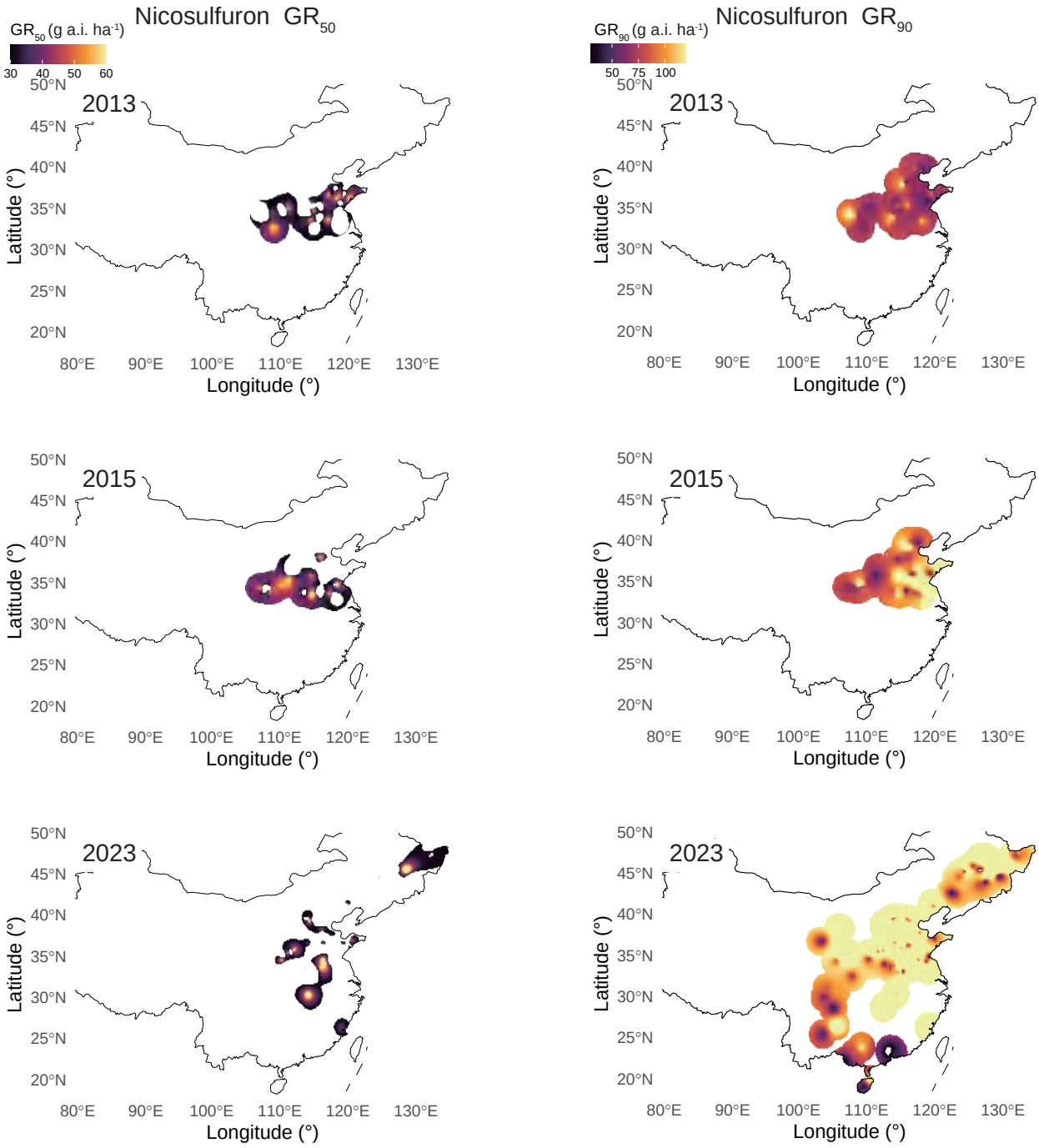

Supplementary Fig. 28 | Geographic distribution of nicosulfuron resistance levels across *Digitaria* accessions. The left panel shows an interpolated heatmap of GR_{50} values for accessions collected in 2013, 2015, and 2023, generated using Inverse Distance Weighting (IDW). The right panel depicts the spatial distribution of relative GR_{90} values.

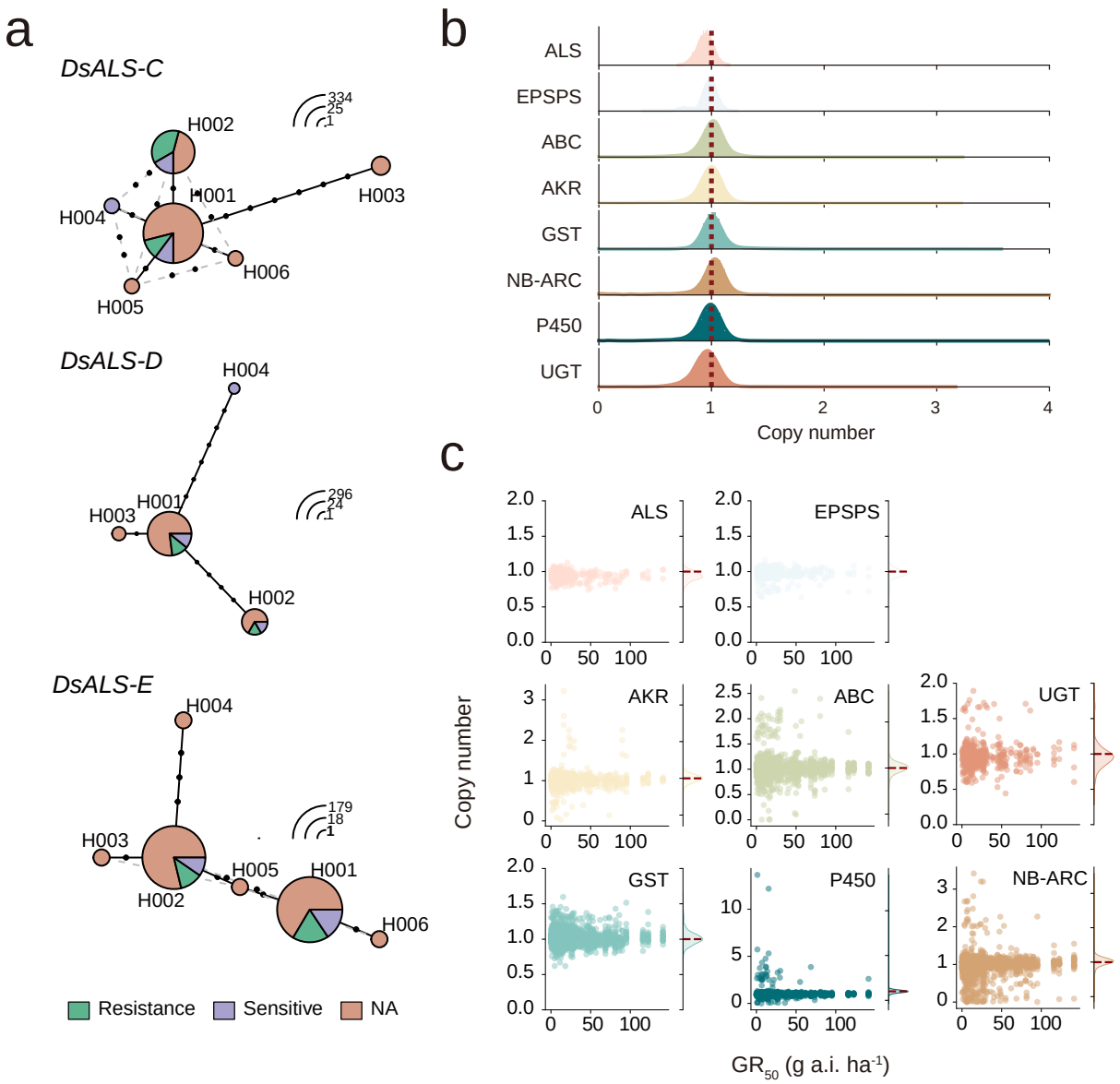

Supplementary Fig. 29 | Haplotype network and copy number variation (CNV) of *DsALS* and associated gene families in *D. sanguinalis* accessions. a, Median-joining haplotype network of *DsALS* copies, with resistance levels indicated by color. **b,** CNV distribution for resistance-associated gene families across all binate *Digitaria* accessions. AKR, Aldo/keto reductase; ALS, Acetolactate synthase; EPSPS, 5-Enolpyruvylshikimate-3-Phosphate Synthase; GST, Glutathione S-transferase; NB-ARC, NB-ARC domain; P450, Cytochrome P450; UGT, UDP-glucoronosyl and UDP-glucosyl transferase; ABC, ABC transporters. **c,** Scatter plot showing the correlation between CNVs of resistance-associated genes and herbicide resistance levels in the accessions.

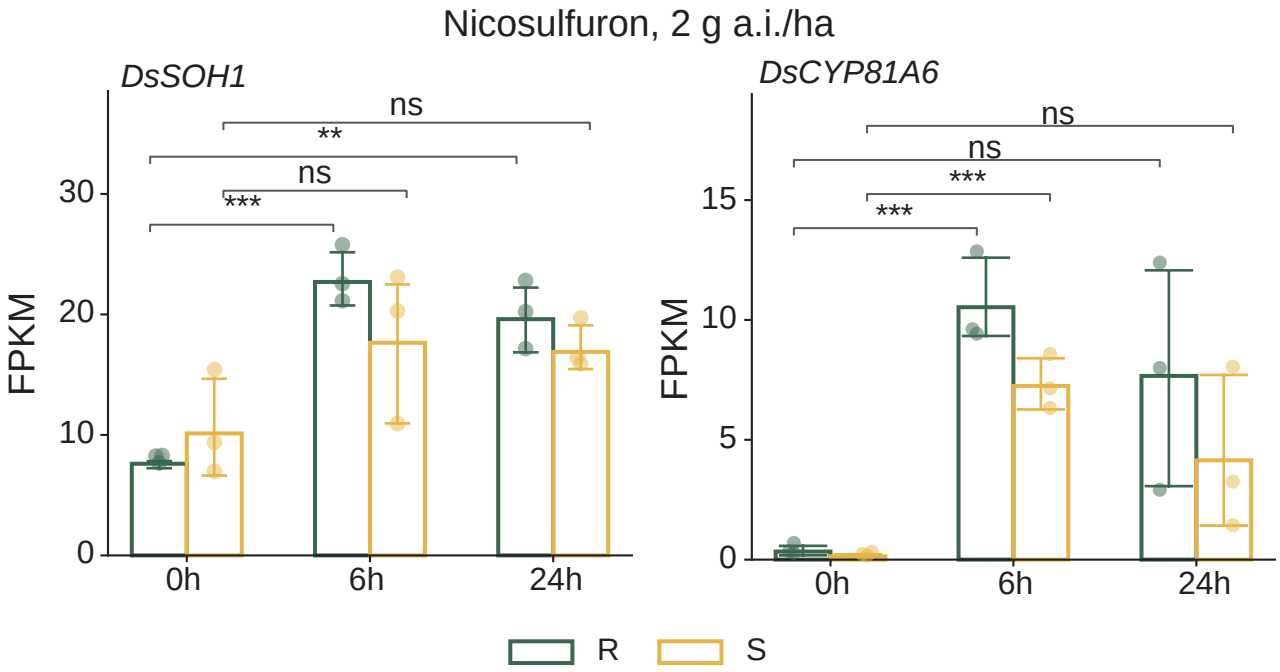

Supplementary Fig. 30 | Expression patterns of resistance-associated genes in resistant (R) and susceptible (S) accessions under nicosulfuron treatment. a, *DsSOH1*. **b,** *DsCYP81A6*. Statistical analysis of these data was performed using the two-tailed *t*-test (*$p < 0.05$, **$p < 0.01$, ***$p < 0.001$).

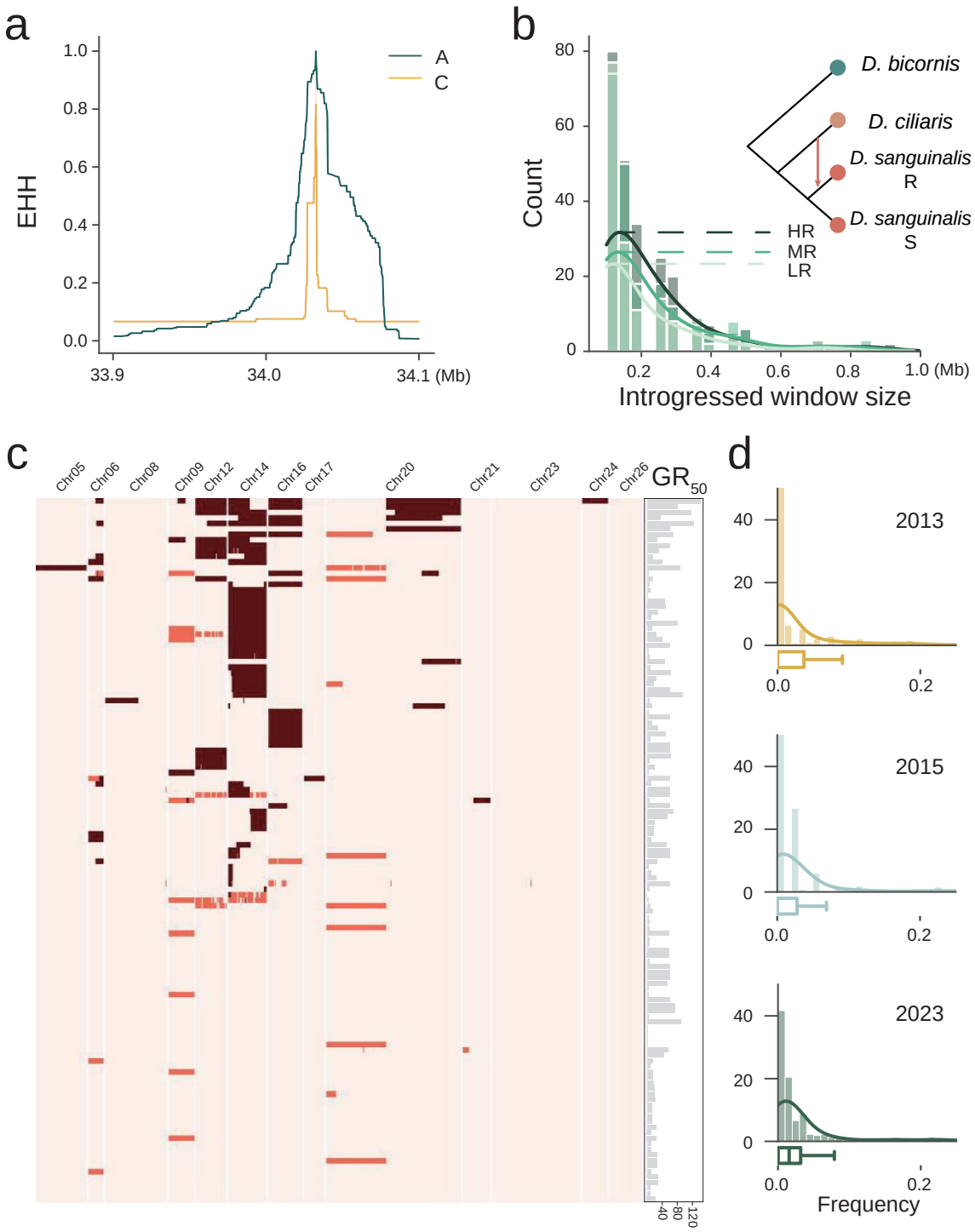

Supplementary Fig. 31 | Introgression analysis in nicosulfuron-resistant populations. **a,** EHH decay for two alternative alleles around Chr20: 34,032,644. **b,** Distribution of introgression windows across populations with differing resistance levels. The top-right panel shows the inferred introgression topology, with red arrows indicating introgression direction from P3 to P2. **c,** *D. ciliaris* haplotype distribution in a 150-kb region surrounding resistance-associated SNPs in hybrid *D. sanguinalis* accessions. The accompanying bar plot displays GR_{50} values. **d,** Frequency distribution of resistance-associated SNPs in accessions collected in 2013, 2015, and 2023.

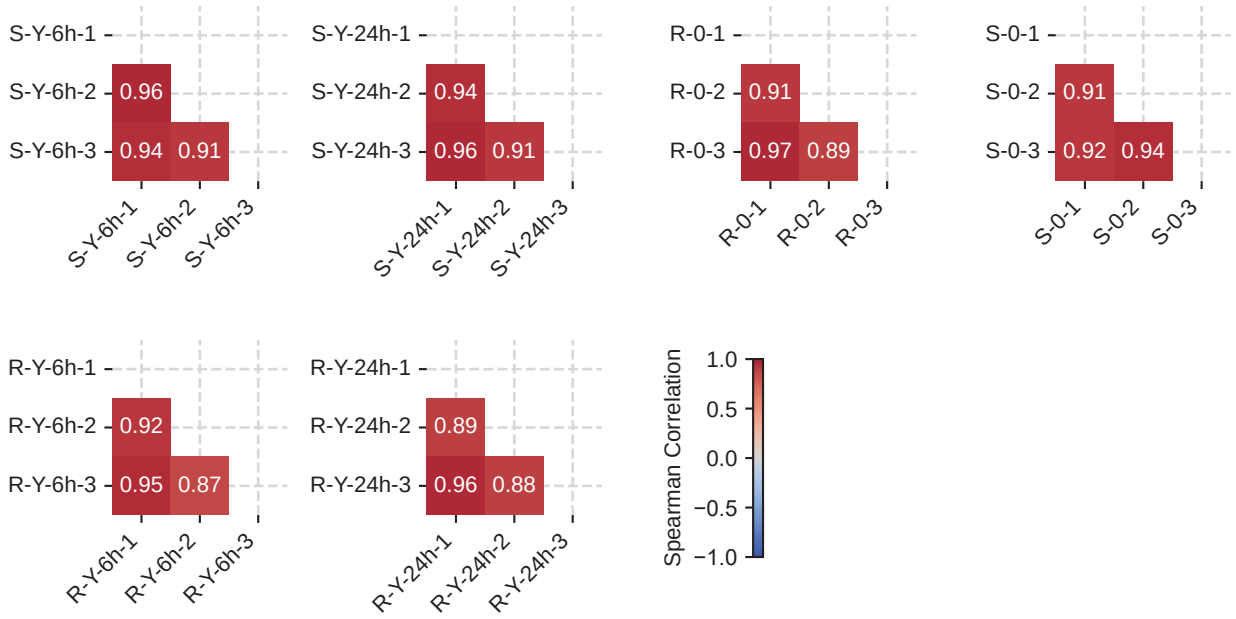

Supplementary Fig. 32 | Heatmap of Pearson correlation coefficients between RNA-seq biological replicates.

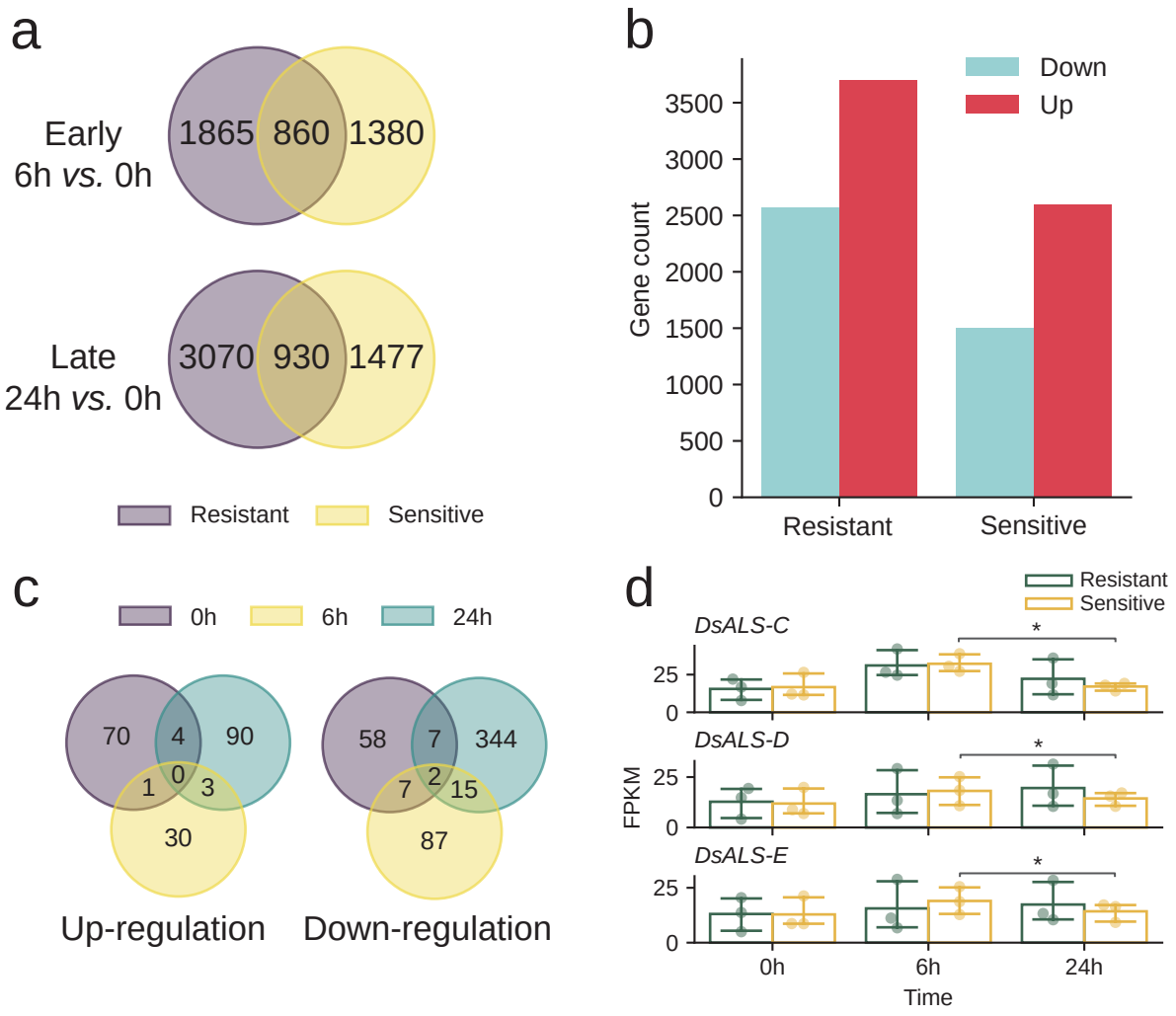

Supplementary Fig. 33 | Differentially expressed gene (DEG) statistics in resistant and susceptible accessions under nicosulfuron treatment. a, Venn diagram showing DEGs in resistant (purple) and susceptible (yellow) accessions. **b,** Numbers of up- and down-regulated DEGs at 6 h vs. 0 h and 24 h vs. 0 h time points. **c,** Venn diagram showing DEGs between resistant and susceptible populations. **d,** Expression patterns of *DsALS* in resistant (R) and susceptible (S) accessions under nicosulfuron treatment. Statistical analysis of these data was performed using the two-tailed *t*-test (*$p < 0.05$, **$p < 0.01$, ***$p < 0.001$). Non-significant comparison was hided.

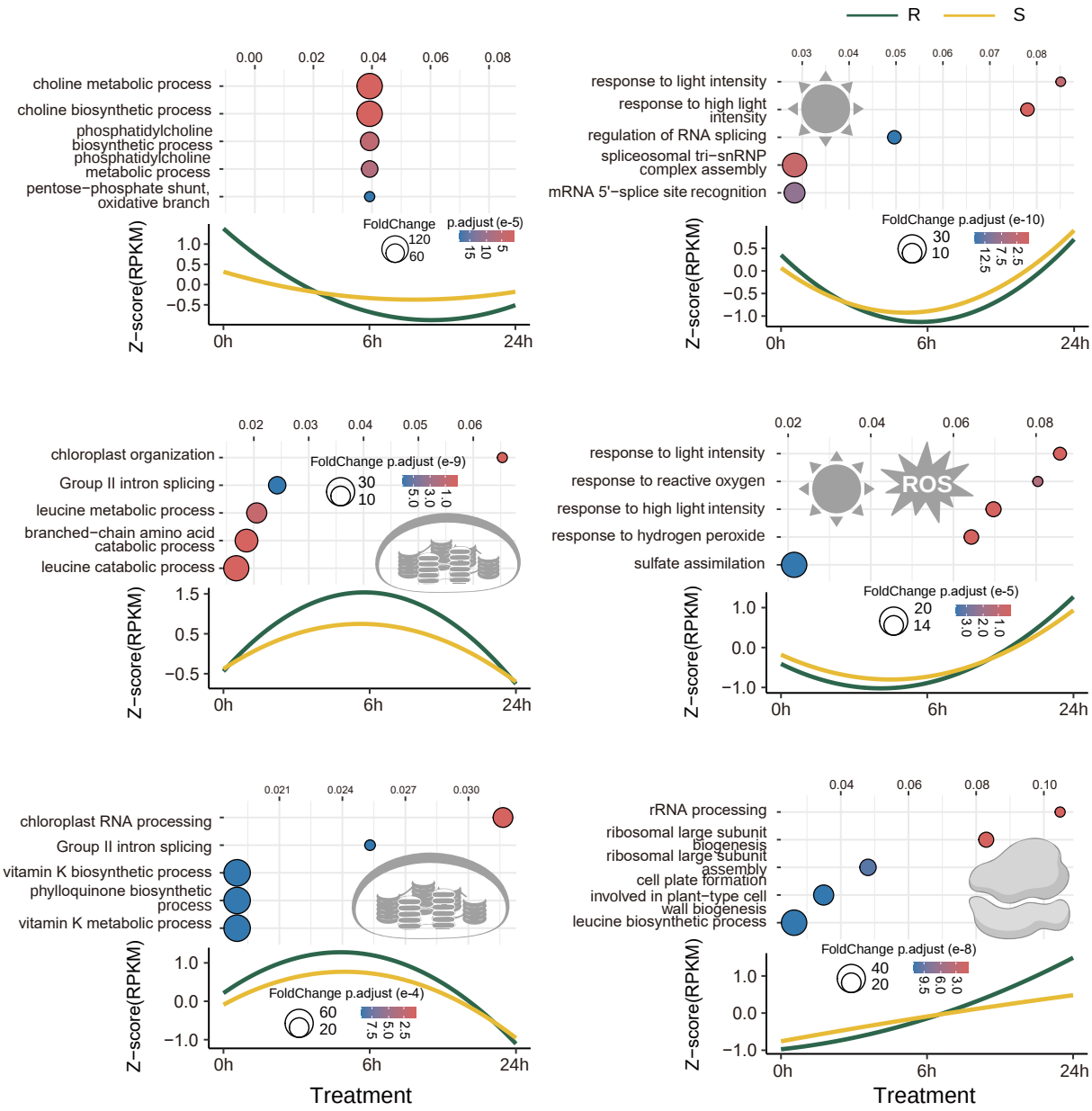

Supplementary Fig. 34 | Clustering of differentially expressed genes in leaf tissues under nicosulfuron treatment, with enrichment of Gene Ontology (GO) terms in biological processes. The top five significantly enriched GO terms (fisher's test, adjusted $p < 0.01$, FDR-corrected) are shown in the upper panel. The lower panel shows expression profiles for resistant (R) and susceptible (S) populations across four representative gene clusters.